



Minerva Access is the Institutional Repository of The University of Melbourne

Author/s:

Groeneveld, J;De Vleeschouwer, D;McCaffrey, JC;Gallagher, SJ

Title:

Dating the Northwest Shelf of Australia Since the Pliocene

Date:

2021-03-01

Citation:

Groeneveld, J., De Vleeschouwer, D., McCaffrey, J. C. & Gallagher, S. J. (2021). Dating the Northwest Shelf of Australia Since the Pliocene. *Geochemistry Geophysics Geosystems*, 22 (3), <https://doi.org/10.1029/2020GC009418>.

Persistent Link:

<https://hdl.handle.net/11343/267317>

License:

[CC BY](#)

# Geochemistry, Geophysics, Geosystems



## RESEARCH ARTICLE

10.1029/2020GC009418

## Dating the Northwest Shelf of Australia Since the Pliocene

### Key Points:

- Independent, orbitally tuned age model for IODP Site U1463
- Correlation of natural gamma radiation and seismic profiling allow a consistent age model for the shelf of northwest Australia
- Independent age model allows updating planktonic foraminiferal biostratigraphy for the Plio-Pleistocene

J. Groeneveld<sup>1,2,3</sup>, D. De Vleeschouwer<sup>4</sup> , J. C. McCaffrey<sup>5</sup> , and S. J. Gallagher<sup>5</sup> 

<sup>1</sup>Alfred Wegener Institute, Helmholtz Center for Polar and Marine Research, Potsdam, Germany, <sup>2</sup>Department of Geosciences, University of Bremen, Bremen, Germany, <sup>3</sup>Now at Center for Earth System Research and Sustainability, Institute for Geology, University of Hamburg, Hamburg, Germany, <sup>4</sup>MARUM-Center for Marine Environmental Sciences, University of Bremen, Bremen, Germany, <sup>5</sup>School of Earth Sciences, The University of Melbourne, Melbourne, Victoria, Australia

### Supporting Information:

- Supporting Information S1

### Correspondence to:

J. Groeneveld,  
[jgroeneveld@uni-bremen.de](mailto:jgroeneveld@uni-bremen.de)

### Citation:

Groeneveld, J., De Vleeschouwer, D., McCaffrey, J. C., & Gallagher, S. J. (2021). Dating the Northwest Shelf of Australia since the Pliocene. *Geochemistry, Geophysics, Geosystems*, 22, e2020GC009418. <https://doi.org/10.1029/2020GC009418>

Received 4 SEP 2020  
 Accepted 21 JAN 2021

**Abstract** Accurate dating of marine sediments is essential to reconstruct past changes in oceanography and climate. Benthic foraminiferal oxygen isotope series from such sediments record long-term changes in global ice volume and deep-water temperature. They are commonly used in the Plio-Pleistocene to correlate deep ocean records and to construct age models. However, continental margin settings often display much higher sedimentation rates due to variations in regional depositional setting and local input of sediment. Here, it is necessary to create a regional multi-site framework to allow precise dating of strata. We create such a high-resolution regional framework to determine the ages of events for the Northwest Shelf (NWS) of Australia, which was cored by International Ocean Discovery Program (IODP) Expedition 356. We employ benthic foraminiferal oxygen and carbon isotopes to construct an astronomically-tuned age model for IODP Site U1463 (5.16–1.69 Ma). The age model is applied to the IODP Site U1463 downhole-logging natural gamma radiation (NGR) depth-series, which was then correlated to NGR depth-series of several IODP sites and industry wells in the area. This approach allows assigning ages to regional seismic reflectors and the timing of key climate-related siliciclastic phases in a predominantly carbonate-rich sequence, like the late Miocene-Pliocene Bare Formation. This age model is also used to chronologically calibrate planktonic foraminiferal biostratigraphic datums showing that the Indonesian Throughflow (ITF) had shoaled enough in the early Pliocene to act as biogeographical barrier between the Pacific and Indian Ocean.

**Plain Language Summary** Determining the age of marine sediments is essential to reconstruct past changes in oceanography and climate. The oxygen isotopes of benthic foraminifera record long-term changes in global ice volume and deep-water temperature, and are commonly used to construct age models. However, continental margin settings often display much higher sedimentation rates due to regional input by rivers. Here, it is necessary to create a regional framework to allow precise dating of strata. We created such a framework for the Northwest Shelf (NWS) of Australia, which was cored by IODP Expedition 356. We used oxygen and carbon isotopes in benthic foraminifera to construct an astronomically-tuned age model for IODP Site U1463. The natural gamma radiation (NGR) variations for IODP Site U1463 were then correlated to those of other IODP sites and industry wells in the area. The IODP Site U1463 age-depth model provides a reference for other archives on the NWS allowing to assign ages to regional seismic reflectors and the timing of sediment input. This age model is also used to determine first and last occurrences of foraminiferal species showing that the Indonesian Throughflow (ITF) blocked the migration of foraminifera from the Pacific to the Indian Ocean after 5 Ma.

## 1. Introduction

Accurate dating of marine sediments is essential to reconstruct past changes in oceanography and climate (Bronk Ramsey, 2009; Huybers & Wunsch, 2004; Lisiecki & Lisiecki, 2002). Global stacks, compilations or splices of long-term oxygen isotope records related to ice volume and temperature are commonly applied to correlate deep ocean records, and to construct age models (De Vleeschouwer et al., 2017; Lisiecki & Raymo, 2005; Zachos et al., 2001). However, for proximal settings with high sedimentation rates such stacks cannot always be used. The supply of large amounts of sediments may dilute the number of microfossils in the sediment to such a degree that geochemical analyses needed to perform the correlation to a global

© 2021. The Authors.

This is an open access article under the terms of the [Creative Commons Attribution License](https://creativecommons.org/licenses/by/4.0/), which permits use, distribution and reproduction in any medium, provided the original work is properly cited.

stack are not possible. Additionally, local or regional climate events may have a big impact on the sediment signal preventing the correlation to a global stack. Under such circumstances it becomes necessary to create a regional framework to allow the accurate construction of age models in that particular area.

The Northwest Shelf (NWS) of Australia is an ideal place to study the effects of global climate and ocean change. It lies directly downstream of the Indonesian Throughflow (a major branch of the global thermohaline conveyor) and is under the direct influence of the Australian Monsoon (Gallagher et al., 2017). The long history of intense hydrocarbon exploration using large seismic and well datasets (Longley et al., 2002) and the recent International Ocean Discovery Program (IODP) Expedition 356 (Gallagher et al., 2017) have revealed the existence of thick (>2 km) sequences of Cenozoic upper bathyal to shelfal marine strata (see summaries in Keep et al., 2018; deMenocal & Gallagher, 2019). These strata record long and short-term climate/ocean variability (Auer et al., 2019; Christensen et al., 2017; De Vleeschouwer et al., 2019, 2018; Gallagher et al., 2009; Groeneveld et al., 2017; Ishiwa et al., 2019; Karatsolis et al., 2020; Moss et al., 2004) and have increased our understanding of reef evolution (Gallagher et al., 2014; Gortler et al., 2002; McCaffrey et al., 2020; Power, 2008; Rosleff-Soerensen et al., 2012; Ryan et al., 2009) and subtropical to tropical siliciclastic/carbonate platform development (Anell & Wallace, 2019; Cathro et al., 2003; Gallagher et al., 2018; Goktas et al., 2016; Sanchez et al., 2012; Tagliaro et al., 2018). In addition, these strata host substantial mass-transport deposits (with volumes ~17 to >162 km<sup>3</sup>) (Hengesh et al., 2013; Scarselli et al., 2013) that were triggered by ongoing neo-tectonism as the Australian plate is colliding with the Asian plate (Keep et al., 2018) or subsidence variability (Gurnis et al., 2020).

Analyses of industry seismic and downhole log datasets/samples have contributed significantly to our knowledge of the Cenozoic evolution of the NWS. However, until IODP Expedition 356 (Gallagher et al., 2017), the only samples of the upper Cenozoic strata of the region were cuttings, sidewall cores (Gallagher et al., 2009; Moss et al., 2004; Rosleff-Soerensen et al., 2012; Wallace et al., 2003), limited engineering cores of the upper 80 m (Collins, 2002; Gallagher et al., 2014) and samples of the modern sedimentary veneer (James et al., 2004; Jones, 1973).

IODP Expedition 356 continuously cored up to 1 km of Miocene to Recent strata in four sites from the Northern Carnarvon and Roebuck basins to document Indonesian Throughflow (ITF) evolution, long-term variations in Australian monsoon precipitation, and the establishment of continental aridity (Gallagher et al., 2017). A suite of downhole logs was obtained from each site including seismic velocity data. These wireline logs are directly comparable to similar data from industry wells (Gallagher et al., 2014) and can be used to correlate subsurface reflectors in 2D seismic data (cf. McCaffrey et al., 2020).

In this work, we construct an astronomically tuned, and, therefore, independent, age model for IODP Site U1463 based on benthic foraminiferal  $\delta^{18}\text{O}$  and  $\delta^{13}\text{C}$  records improving the accuracy and temporal resolution of previous age models for this site (Auer et al., 2019; Christensen et al., 2017; De Vleeschouwer et al., 2018; Karatsolis et al., 2020). We then extrapolate the IODP Site U1463 age model to other IODP Expedition 356 sites, as well as to regional industry wells and to 2D seismic data. This approach ultimately results in a consistent age model for late Neogene strata on the NWS of Australia. The correlation of Neogene stratigraphy among industry wells and IODP Expedition 356 sites is achieved by using natural gamma radiation (NGR) wireline logs. Distinct marker beds and their geological ages are then mapped throughout regional 2D seismic lines along the NWS. The independent age model is also used to establish a high-resolution planktonic foraminiferal biostratigraphy allowing comparison with published biohorizons from the latest Miocene into the Pleistocene. These updated, calibrated biohorizons will help to disentangle planktonic foraminiferal paleobiogeographic patterns related to the Indonesian Throughflow by comparison with sites located in the western Pacific and the rest of the Indian Ocean for the Neogene.

## 2. Material and Methods

### 2.1. Site Selection

We selected a series of IODP sites and industry wells to establish a consistent framework for dating the NWS (Figure 1; Table 1). IODP Site U1463 in the Northern Carnarvon Basin was selected as reference site

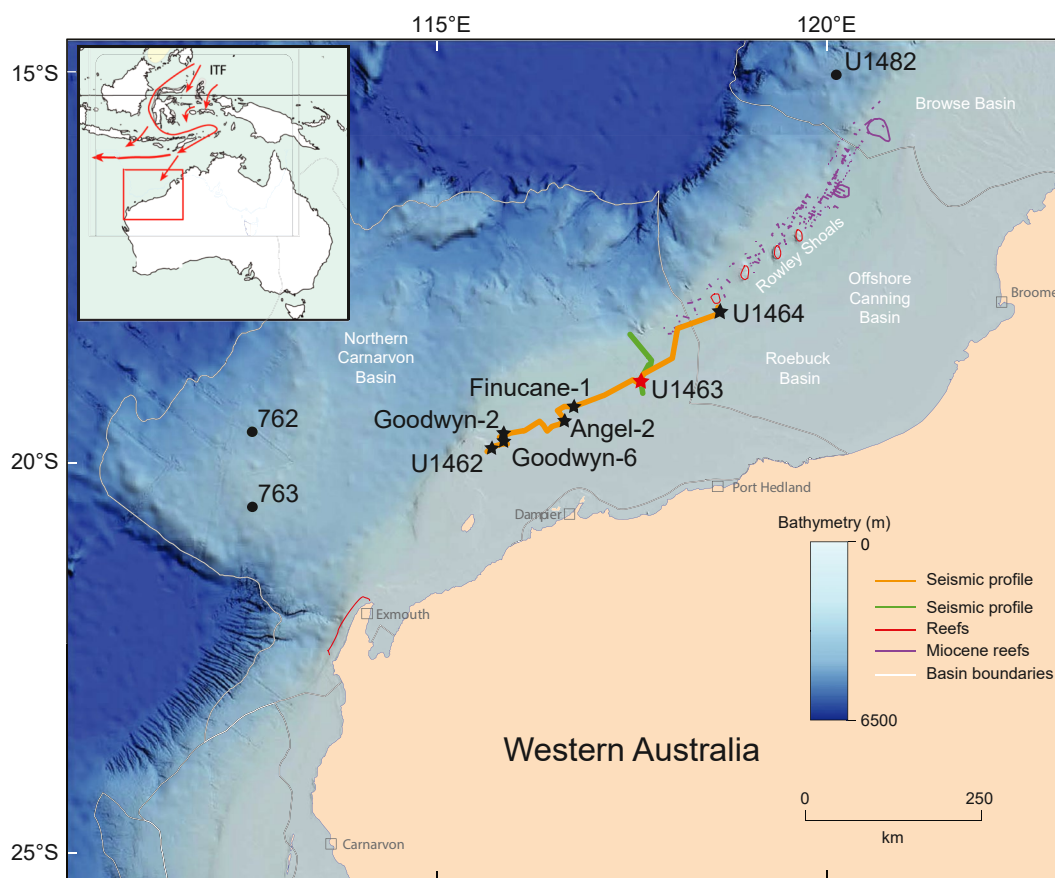


**Figure 1.** Map of the northwest shelf of Australia with relevant IODP and ODP sites and industry wells used in this study (black stars) with IODP Site U1463 as reference site (red star). Additional sites discussed in the text are also indicated (black dots). Orange line indicates the seismic profile connecting the different site locations; green line depicts the downslope profile including IODP Site U1463. Additional main features of the NWS like basin boundaries, existing and paleo-reefs are marked. Inset shows the study area with respect to the Indonesian Throughflow (ITF). IODP, International Ocean Discovery Program; NWS, Northwest Shelf.

**Table 1**  
Overview of IODP Sites and Industry Wells Used in This Study

Site	IODP exp. 356	Industry well	Latitude	Longitude	Present-day water depth (m)
U1462C <sup>a</sup>	X	–	19°49.28'S	115°42.62'E	87
U1463B <sup>b</sup>	X	–	18°57.92'S	117°37.43'E	145
U1464C	X	–	18°03.92'S	118°37.89'E	264
Finucane-1	–	X	19°17.34'S	116°45.96'E	139
Angel-2	–	X	19°27.90S	116°39.48'E	87
Goodwyn-6	–	X	19°43.32'S	115°51.30'E	124
Goodwyn-2	–	x	19°39.78'S	115°51.96'E	133

IODP, International Ocean Discovery Program.

<sup>a</sup>Within 150 m of Fisher-1 industry well. <sup>b</sup>Within 150 m of Picard-1 industry well.

for the NWS of Australia as this site contains a continuous, high-resolution record of deeper water sediments from the Mio-Pliocene transition into the Pleistocene (Gallagher et al., 2017). A high-resolution benthic stable oxygen and carbon isotope record was established for this site and astronomical tuning was performed to provide an independent age model for the NWS. The NGR record was then used for correlation to the other IODP sites and the industry wells. Additionally, this age model was used to determine the timing for important biostratigraphic datums for planktonic foraminifera for this section of the Indian Ocean.

IODP Site U1462 in the Northern Carnarvon Basin and IODP Site U1464 in the Roebuck Basin are included as part of a parallel section along the NWS (Figure 1). For all these sites NGR records are available and can therefore be correlated to the reference NGR record of IODP Site U1463 (Gallagher et al., 2017). Additionally, we included a series of industry wells on the NWS to expand the coverage on the NWS (Figure 1; Table 1). The wells were selected based on their previous use in paleoceanographic reconstructions, and for having representative NGR records to allow correlation with the IODP sites (Gallagher et al., 2014).

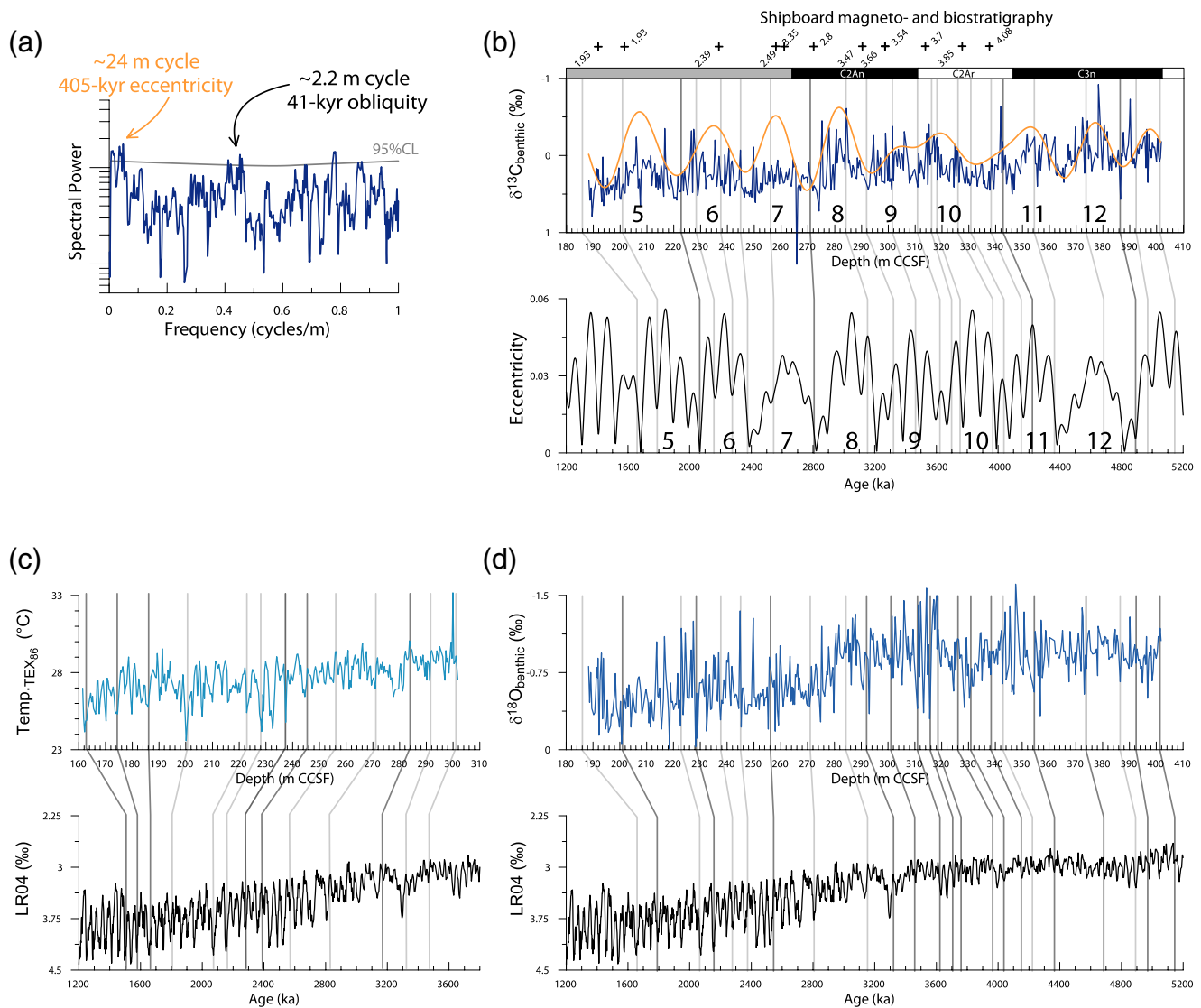


**Figure 2.** Determination of dominant cyclicty and tie-points in the records of IODP Site U1463. (a) Spectral analysis of the  $\delta^{13}\text{C}_{\text{benthic}}$  record of IODP Site U1463 in the depth domain reveals significant cycles at  $\sim 2.2$  and  $\sim 24$  m; (b) Shipboard-based magneto- and biostratigraphy allow identification of 405-kyr eccentricity cycles and initial age model related to the orbital solution (Laskar et al., 2004). Black crosses indicate shipboard calcareous nannofossil and planktonic foraminiferal biostratigraphic age markers (Gallagher et al., 2017); (c) Correlation of the  $\text{TEX}_{86}$  record (Smith et al., 2020) in the depth domain with the benthic  $\delta^{18}\text{O}$ -stack LR04 (Lisiecki & Raymo, 2005); (d) Correlation of the benthic  $\delta^{18}\text{O}$  in the depth domain with the benthic  $\delta^{18}\text{O}$ -stack LR04 (Lisiecki & Raymo, 2005). Gray, vertical lines between the records in panels b–d indicate tie-points; dark gray lines indicate tie-points based on the proxy in that particular panel. IODP, International Ocean Discovery Program.

## 2.2. Benthic Stable Oxygen and Carbon Isotopes

The shipboard biostratigraphy (Christensen et al., 2017; Gallagher et al., 2017) provided the necessary time markers to inform a sampling strategy that allows for the construction of an astronomically-tuned age model (30–40 cm sampling resolution, corresponding to  $\sim 6$  kyr temporal resolution; Figure 2). Samples were freeze-dried, subsequently washed over a  $63\ \mu\text{m}$  mesh sieve and oven-dried. As preservation was occasionally poor and abundance low we selected *Uvigerina* spp. instead of one species of *Uvigerina* for performing stable oxygen and carbon isotopes (Figures 2 and 3). Up to 20 specimens were picked from the 250–400  $\mu\text{m}$  size fraction, which was extended to 150–250  $\mu\text{m}$  when not enough specimens were present. Stable isotope analyses were performed on a Finnigan MAT 251 gas isotope ratio mass spectrometer equipped with an automated carbonate preparation device at MARUM, University of Bremen. Isotopic results were calibrated

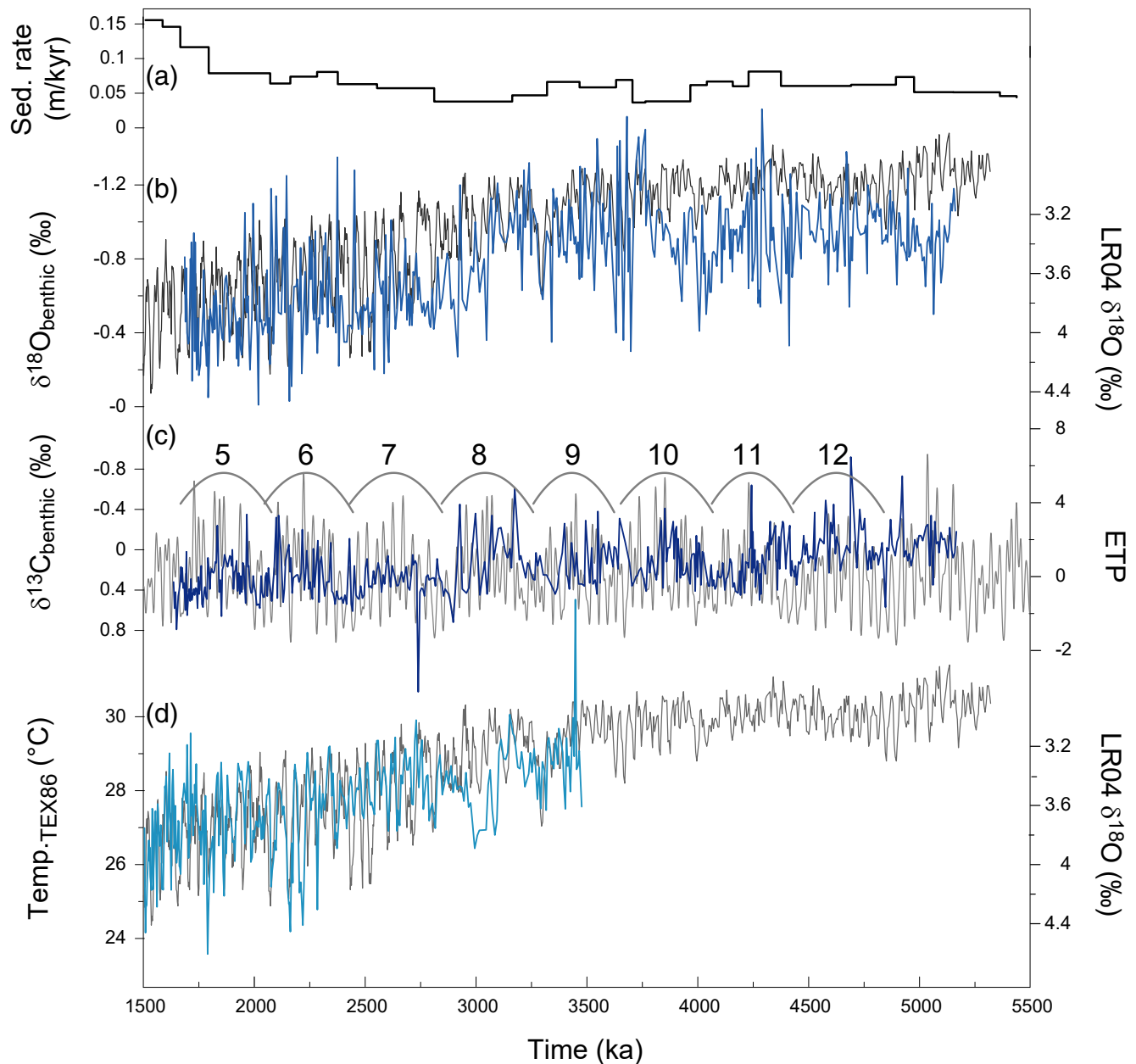


**Figure 3.** Construction of the astronomically-tuned age model for IODP Site U1463. (a) Sedimentation rate resulting from the new age model; (b) The  $\delta^{18}\text{O}_{\text{benthic}}$  record of IODP Site U1463 (blue) using *Uvigerina* spp. in comparison with the global benthic LR04  $\delta^{18}\text{O}$ -stack (black) (Lisiecki & Raymo, 2005); (c) the  $\delta^{13}\text{C}_{\text{benthic}}$  record of IODP Site U1463 (blue) in comparison with ETP (black) (eccentricity—tilt—precession; Laskar et al., 2004); (d)  $\text{TEX}_{86}$  temperatures for Site U1463 (blue) (Smith et al., 2020) in comparison with the global benthic LR04  $\delta^{18}\text{O}$ -stack (black) (Lisiecki & Raymo, 2005). IODP, International Ocean Discovery Program.

relative to the Vienna Pee Dee belemnite (VPDB) using the NBS19 standard. The standard deviation of the house standard (Solnhofen limestone) was 0.03‰ for  $\delta^{13}\text{C}$  and 0.04‰ for  $\delta^{18}\text{O}$  during the measuring period.

### 2.3. Spectral Analyses

Spectral analyses were carried out using the multi-taper method with three  $2\pi$ -tapers (Thomson, 1982) and LOWSPEC background estimation (Meyers, 2012), as implemented in the R-package “astrochron” (Meyers, 2014). The confidence levels were calculated applying the LOWESS-based procedure (Cleveland, 1979; Ruckstuhl et al., 2001). Depth-to-time conversion and bandpass filtering were carried out using the functions

“tune” and “bandpass” from the same R-package. The astronomical solution of Laskar et al. (2004) was used as reference (Figure 2). Generally, this study adheres to the guidelines for an effective cyclostratigraphic study described in Sinnesael et al. (2019).

#### 2.4. Biostratigraphy

Dried samples were sieved at 150  $\mu\text{m}$  mesh before identification of specific marker species. A total of 121 samples of IODP Site U1463 (section 356-U1463-C-20-H4 (188.05 m CCSF) to section 356-U1463-C-56-F3 (401.78 m CCSF)) were investigated for specific species of planktonic foraminifera to determine if biostratigraphic first and/or last occurrences agree with published datums for the Atlantic and Pacific. Planktonic foraminifera were identified following the taxonomy of Kennett and Srinivasan (1983), Bolli and Saunders (1985), Schiebel et al. (2017), Wade et al. (2018), and Lam and Leckie (2020a). Published ages for bio-events are from Wade et al. (2011) and King et al. (2020). Individual foraminifera were recorded in qualitative terms based on an assessment of all grains from the 150 to 250  $\mu\text{m}$ , 250 to 400  $\mu\text{m}$ , and  $>400$   $\mu\text{m}$  size fractions loosely covering a picking tray. The relative abundance of specific foraminiferal species within the assemblage was classified as common, possibly present, or in absolute numbers to determine ratios (e.g., sinistral vs. dextral for *Pulleniatina* spp.). Due to the occasional poor preservation of the sample material, it was not always possible to determine if a certain species was present in a particular sample (Gallagher et al., 2017). Preservation was classified from very poor via poor, medium, and good to very good.

#### 2.5. Dynamic Time Warping of Natural Gamma Radiation Records

Downhole logging formed an indispensable part of scientific data acquisition during IODP Expedition 356, with downhole logging performed at five out of a total of seven sites (Gallagher et al., 2017). In this paper, we incorporate downhole logging records from IODP sites U1462, U1463 (Northern Carnarvon Basin) and U1464 (Roebuck Basin). The natural gamma radiation (NGR) logs of the latter two sites have been used for paleoclimate studies in Christensen et al. (2017) and Groeneveld et al. (2017) respectively, and a detailed description of the NGR downhole logging methodology during IODP Expedition 356 can be found in these two studies.

We complement the IODP NGR downhole logs with wireline log data from the latest Miocene to Pleistocene sections of four industry wells from the Northern Carnarvon Basin (Figures 1 and 4; Table 1). From east to west, these industry wells are Finucane-1, Angel-2, Goodwyn-6, and Goodwyn-2; their well logs can be sourced from the Geoscience Australia online NOPIMS database (<http://www.ga.gov.au/nopims>; last access May 21, 2020). We interpreted the approximate stratigraphic position of the latest Miocene in the industry wells by using previously-published biostratigraphic data from cuttings by Gallagher et al. (2009, 2014) and by extrapolating from the detailed IODP age-depth models in the Carnarvon Basin.

We established a detailed correlation between the three IODP and four industry NGR downhole logs by applying a dynamic time warping approach. Dynamic time warping (DTW) is a technique to compare depth- or time-series with each other (Figure 5; supporting information). The objective of DTW is, given two complementary series, to stretch or compress them locally in order to make one resemble the other as much as possible. Hence, the warping refers to the optimal deformation of the depth- or time-scale of one of the two input series to match the other. It is important to note that DTW results in a continuous transfer function between the warped and the reference record. It thus does not provide specific tie-points linking the analyzed records. In a geologic context, DTW can be useful, as the technique can incorporate constraints on stratigraphic ages and realistic sedimentation rates (Kotov & Pälke, 2017; Lisiecki & Herbert, 2007; Lisiecki & Lisiecki, 2002). In this study, we compute dynamic time warps and optimal alignments between NGR-logs by using the open-source R package *dtw* by Giorgino (2009) on the R platform for statistical computing (R Core Team, 2014). Thereby, we always use the IODP Site U1463 computed gamma ray emission (HCGR) measured in American Petroleum Institute units (gAPI) as the reference. The depth-scales of the two other IODP sites and four other industry wells are thus warped to display an optimal NGR-series fit with IODP Site U1463 (Figures 4 and 5; supporting information). During DTW, we use the slope-constrained step patterns from Sakoe and Chiba (1978) to place bounds on the local slope of the warping curve. Therefore, we avoid the situation where local sedimentation rates exhibit unrealistic deviations from the mean sedimentation

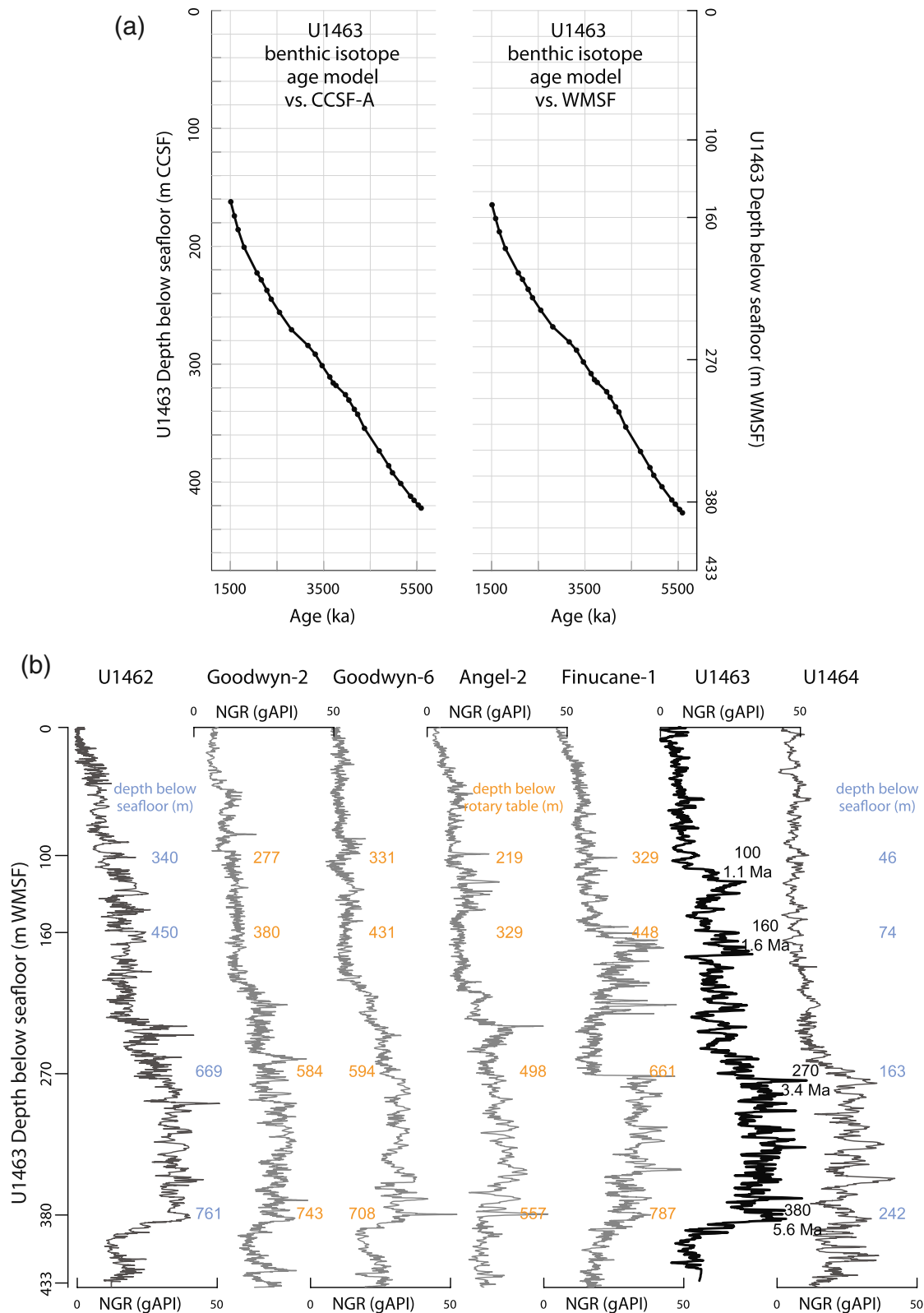


**Figure 4.** Correlation of the NGR record of IODP Site U1463 with other IODP sites and industry wells. (a) Sediment depth (m WMSF and m CCSF) versus age according to the new age model for IODP Site U1463; (b) NGR comparison based on the NGR record of IODP Site U1463 plotted versus sediment depth (m WMSF). The NGR records of the other sites are plotted according to their correlation to the IODP Site U1463 NGR record. The numbers along the respective record indicate the depth in those records where that particular depth correlates to the same feature in the NGR record of IODP Site U1463 (in meters below sea floor/rig floor). IODP, International Ocean Discovery Program; NGR, natural gamma radiation.

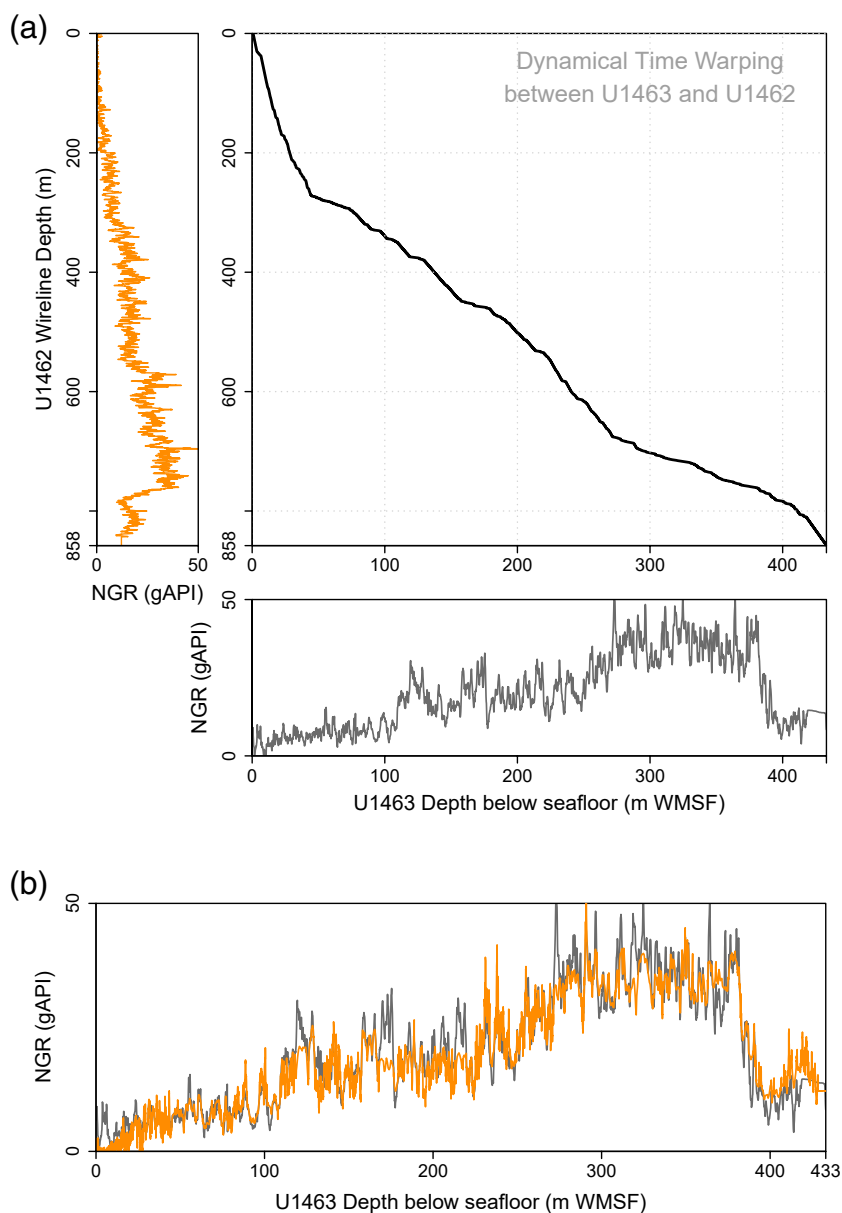


**Figure 5.** (a) Dynamical time warping between the reference IODP Site U1463 NGR record and the NGR record of IODP Site U1462 (see supplements for the warping with the other sites); (b) Resulting correlation between IODP sites U1463 (black) and U1462 (orange) showing the good match between both NGR records. IODP, International Ocean Discovery Program; NGR, natural gamma radiation.

rate. After DTW, we tested whether the generated mapping function between the depth-series under investigation and IODP Site U1463 fulfills biostratigraphic and lithostratigraphic scrutiny. When this was not the case, we reiterated DTW with adjusted settings, for example by tightening or relaxing sedimentation rate constraints or by adjusting the presumed stratigraphic position of the latest Miocene in the industry wells.

## 2.6. Definition of Different Depth Scales

The measurement of depth is an essential obstacle in sub-surface marine geology. Next to the two-way travel time in seismic images, this study uses several different depth-scales for isotopic and NGR depth-series following commonly used routines for the respective data sources. Industry wireline NGR logs are reported along a depth-scale in meters below rotary table (mbrt) from which the well was drilled. This depth scale

thus also includes the full depth-range of the water column and the height of the rotary table above mean sea-level. Sources of error in this depth-scale are related to uncompensated heave in case of floating rigs, stretching of the wireline cable and stick and slip of the downhole tool.

IODP wireline NGR logs are reported using a Wireline log Matched depth below Sea Floor (WMSF) depth scale. Water depth and rig height are excluded by identifying the sea floor by means of a stepwise increase in the NGR signal at the sea bed. The uncertainty on this determination adds to the above-mentioned sources of error.

Core-based data from the IODP sites, like the biostratigraphic horizons, are reported in cored meters below seafloor (CSF-A). Each hole of a particular site has its own CSF-A depth scale. Additionally to the wireline downhole logging to acquire the NGR, discrete analyses for NGR were also performed on the recovered core material (Christensen et al., 2017; Gallagher et al., 2017). This allowed to correlate between the CSF-A depth scale (discrete NGR analyses) and the WMSF depth scale of the downhole logging (Christensen et al., 2017). The resulting tie-points were used to linearly extrapolate from the CSF-A depth scale to the WMSF depth scale.

We report benthic isotope data, measured on IODP core samples, along the Core Composite depth below Sea Floor (CCSF) depth scale. This depth scale considers adjusted depths constructed to resolve gaps in the core recovery and depth inconsistencies between the different holes and their respective CSF-A depth scales. Typically, a CCSF scale is constructed onboard a research vessel like R/V *JOIDES Resolution* by shifting cores vertically based on the correlation of high-resolution core logging data from multiple, adjacent holes. In this instance, for IODP Site U1463, we use the shipboard splice (Gallagher et al., 2017), with the slight revision in the Pliocene, as reported in De Vleeschouwer et al. (2018). At IODP Site U1463, the WMSF depth is consistently shallower than the CCSF scale: The offset between wireline and coring depth varies from 15 to 38 m and may be explained by sediment expansion in the drilling process.

### 2.7. Seismic Correlation and Age Determination

Extensive publicly released petroleum exploration multichannel seismic surveys are available for the NWS for our 2D seismic analyses (Longley et al., 2002), which have been provided by Geoscience Australia (<https://nopims.dmp.wa.gov.au/nopims>; latest access June, 7 2020). These industry seismic data have been extensively used in previous studies to document the Paleogene to Neogene evolution of the carbonates and siliciclastics along this margin (e.g. Belde et al., 2017; McCaffrey et al., 2020; Rosleff-Soerensen et al., 2012). Key seismic reflectors in these datasets were previously assigned ages based on either biostratigraphy (Belde et al., 2017; Gallagher et al., 2014; McCaffrey et al., 2020) or Sr-isotope ages (Rosleff-Soerensen et al., 2012). In this study we use the ages determined by the orbitally-tuned benthic foraminiferal isotope age model.

We constructed two composite seismic profiles; one parallel along the NWS connecting the different IODP sites and industry wells, and one perpendicular to IODP Site U1463 to show the 3D-presence of the main features on the NWS (Figures 6 and 7). The WMSF depth scale was converted to a two-way travel time (TWT) scale using downhole velocity (check-shot) data to allow the ages to be plotted on seismic profiles. In the absence of check-shot velocity data, correlation to the TWT scale is calculated by cumulatively adding sonic travel times between each downhole P-wave velocity measurement. Industry well depths were correlated to the TWT scale using the calibrated check-shot data and Vertical Seismic Profiles (VSP) from Industry well completion reports. Seismic correlation and identification of characteristic features were performed using the IHS Markit Kingdom software using standard criteria for identification (Mitchum Jr. et al., 1977). The characteristic horizons H5 (Tortonian), H6 (Base Pliocene), and H7 (Base Pleistocene) were used as baseline to correlate the different seismic profiles (Belde et al., 2017; McCaffrey et al., 2020).

## 3. Results and Discussion

### 3.1. Orbitally Tuned Age Model Based on Benthic Stable Isotopes

The initial age model for IODP Site U1463 was based on shipboard data, specifically the biostratigraphy using nannofossils and planktonic foraminifera (Christensen et al., 2017; Gallagher et al., 2017). This showed that a complete latest Miocene to Pleistocene sediment sequence is present at IODP Site U1463. Stable

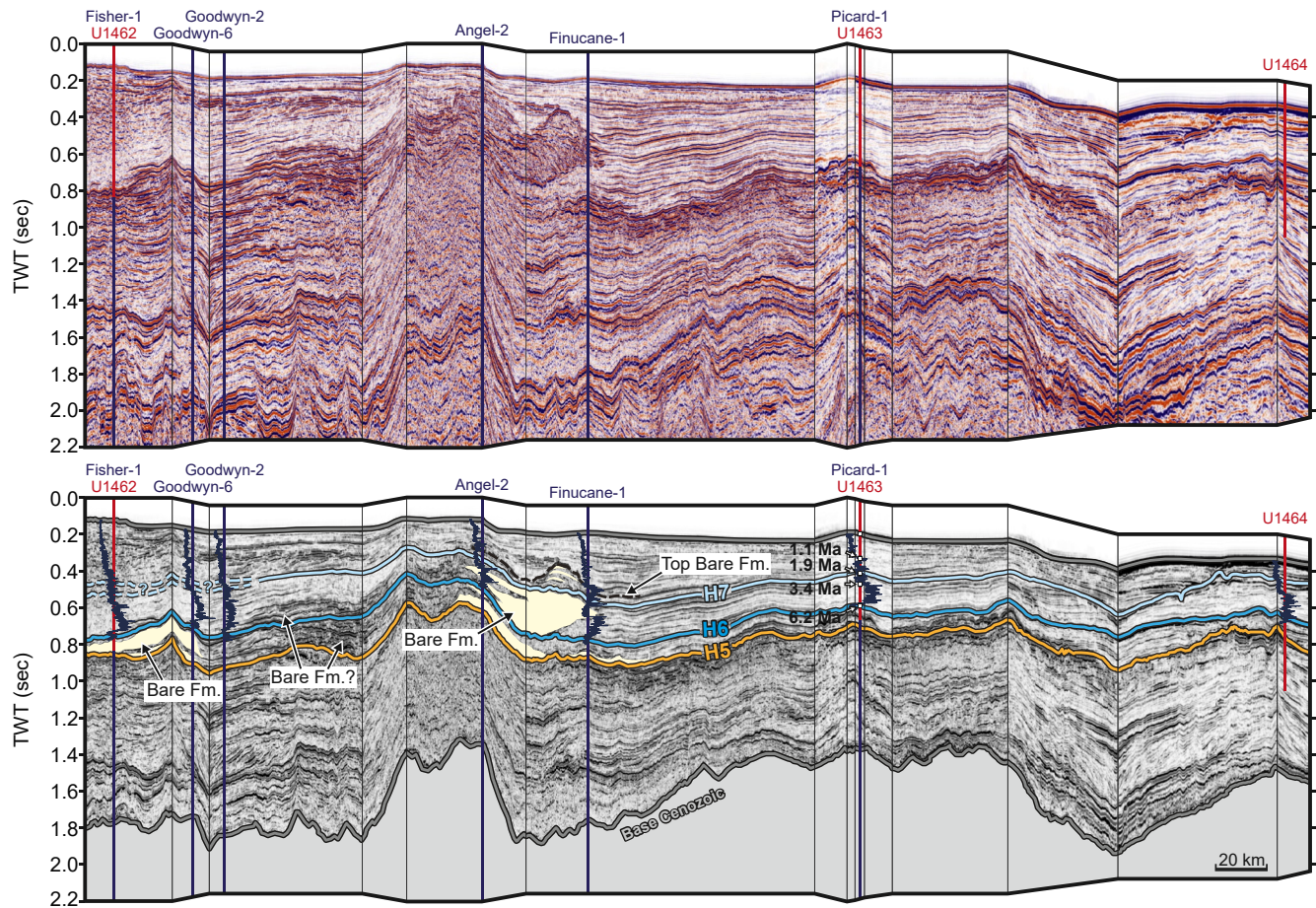


**Figure 6.** Alongshore seismic profile from IODP Site U1462 to IODP Site U1464 showing that the main seismic reflectors during the late Neogene can be followed along the NWS. The reflectors Base Cenozoic and H1-H7 are based on Belde et al. (2017) and McCaffrey et al. (2020) with updated ages for H6 and H7. The Base Cenozoic reflector is used in the industry as a consistent standard reflector for the NWS. An estimation of siliciclastic deposits of the Bare Formation is marked (white) showing its non-synchronous deposition on the NWS; the top of the formation follows the interpretation of Tagliaro et al. (2018). The NGR records at the respective core locations are shown in blue for comparison with the seismics including the ages for reflectors H6 and H7 and specific depth markers as indicated in Figure 4. Thin vertical lines indicate where the composite seismic profile moved from one individual seismic line to another parallel one. IODP, International Ocean Discovery Program; NGR, natural gamma radiation; NWS, Northwest Shelf.

oxygen and carbon isotopes using the planktonic foraminifer *Trilobatus sacculifer* showed that the  $\delta^{13}\text{C}$  record exhibited the 405 kyr eccentricity cyclicity that could be correlated to the astronomical solution (De Vleeschouwer et al., 2018; Laskar et al., 2004). The completeness of the IODP Site U1463 sediment archive and its clear link to global insolation patterns means it can be used to construct a reference age model for the NWS of Australia.

Benthic stable oxygen isotope data are commonly used to construct Plio-Pleistocene age models as they contain the global signature of climatic and oceanographic change through time (Lisiecki & Raymo, 2005). The main premise of these type of data is that the benthic foraminifera live at water depths where local changes in water mass characteristics are only minor, and thus the global signal is the main control on this proxy. Paleo-water depths for IODP Site U1463 during the Pliocene and early Pleistocene, however, were never deeper than ~600 m, which means that bottom waters may have experienced significant changes in temperature and salinity affecting the  $\delta^{18}\text{O}$ -signature of benthic foraminifera (Gallagher et al., 2017; Gurnis et al., 2020). Additionally, ice volume changes during the early Pliocene, and thus variations in benthic  $\delta^{18}\text{O}$ , were not very pronounced (Lisiecki & Raymo, 2005). Spectral analysis of the *Uvigerina* spp.  $\delta^{13}\text{C}$  record in the depth domain shows the presence of significant cycles of ~2.2 m and ~24 m, respectively (Figure 2). Taking into account bio- and magnetostratigraphic constraints, these cycles likely correspond to the imprint of 41-kyr obliquity and 405-kyr eccentricity. The latter cycles are particularly useful for age-depth model

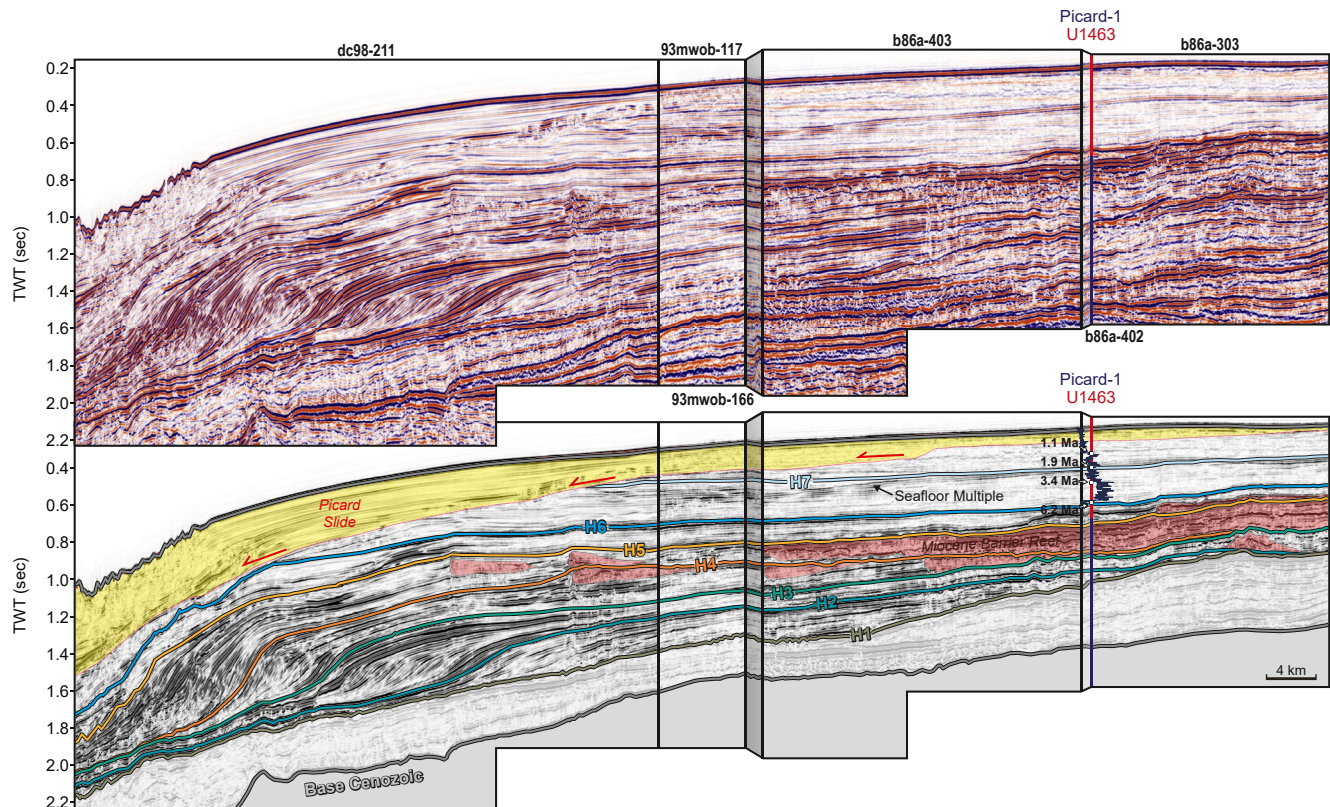


**Figure 7.** Seismic profile perpendicular to the seismic profile in Figure 6 anchored at the location of IODP Site U1463 showing the continuation of the main reflectors downslope, Miocene reefal carbonates previously identified by McCaffrey et al. (2020), and the newly appointed Picard slide covering the underlying sediment sequence. The NGR record of IODP Site U1463 is shown for comparison with the seismics including the ages for reflectors H6 and H7 and specific depth markers as indicated in Figure 4. IODP, International Ocean Discovery Program; NGR, natural gamma radiation.

construction, as the bio- and magnetostratigraphy unambiguously assigns them to the fifth–twelfth 405-kyr eccentricity cycles counting back from the present (Figure 2; Laskar et al., 2004). In this first step, we thus applied the 405-kyr astrochronozones as proposed by Hilgen et al. (2020). In a second step, we correlated the benthic  $\delta^{18}\text{O}$  record at IODP Site U1463 to the LR04 benthic oxygen isotope stack for pinpointing the more pronounced glacial cycles (Figure 3; Lisiecki & Raymo, 2005). In the younger part of the age model, that is after the onset of Northern Hemisphere Glaciation (<2.7 Ma), we additionally used the strong expression of glacial-interglacial oscillations in the  $\text{TEX}_{86}$  sea water temperature record of IODP Site U1463 to fine-tune the age model (Smith et al., 2020). The 29 tie-points between depth and time define the age-depth model of IODP Site U1463 and imply sedimentation rates between 4 and 8 cm/kyr throughout the studied interval with increasing sedimentation rates up to 16 cm/kyr in the youngest part of the record (Table 2). The age model in this study is similar yet temporally more extensive (~3.5 Myr vs. < 1 Myr) than the previous IODP Site U1463 age models presented in De Vleeschouwer et al. (2018) and Auer et al. (2019).

### 3.2. Planktonic Foraminiferal Biostratigraphy

Biostratigraphy using planktonic foraminifera is important not only for paleoceanographic reconstructions but also commonly used in the industry for age dating of petroliferous strata. The first and last appearances of different species, known as biohorizons, can be linked to paleomagnetic timescales and orbitally tuned using benthic foraminiferal  $\delta^{18}\text{O}$  records to create highly precise age models (Gradstein et al., 2012; Wade et al., 2011). The initial age models for IODP Site U1463 and the nearby IODP sites were only based on the biostratigraphy, as the nature of the carbonate-rich sediments present prevented reliable paleomagnetic analyses (Gallagher et al., 2017). However, not all of these biohorizons are globally synchronous. Isolated basins like the Mediterranean, tectonic obstructions like the closing of oceanic gateways, or climate-induced

**Table 2**

*Tie-points of Reconstructed Age versus Sediment Depth and Sedimentation Rates Based on Benthic Stable Oxygen and Carbon Isotopes,  $TEX_{86}$  Temperatures (Smith et al., 2020), and K (%) (Christensen et al., 2017; Karatsolis et al., 2020) of IODP Site U1463*

Depth (m WMSF)	Depth (m CCSF)	Age (ka)	Sedimentation rate (m/kyr)	Reference proxy
150.22	162.23	1,509.36	–	$TEX_{86}$
160.84	174.20	1,586.37	0.16	$TEX_{86}$
171.05	185.84	1,666.14	0.15	$TEX_{86}$
183.98	200.76	1,794.32	0.12	$\delta^{18}O$
202.84	222.61	2,071.61	0.08	$\delta^{13}C$
207.87	228.43	2,162.55	0.06	$\delta^{18}O$
215.57	237.34	2,283.15	0.07	$TEX_{86}$
222.08	244.87	2,376.48	0.08	$TEX_{86}$
231.74	256.04	2,553.57	0.06	$\delta^{18}O$
244.58	270.79	2,811.28	0.06	$\delta^{13}C$
256.21	284.14	3,163.08	0.04	$TEX_{86}$
262.64	291.51	3,320.15	0.05	$\delta^{18}O$
271.75	301.23	3,466.79	0.07	$\delta^{18}O$
280.76	310.86	3,631.48	0.06	$\delta^{18}O$
285.54	315.97	3,705.36	0.07	$\delta^{18}O$
287.54	318.10	3,763.68	0.04	$\delta^{18}O$
294.79	325.85	3,966.33	0.04	$\delta^{18}O$
299.10	330.44	4,040.77	0.06	$\delta^{18}O$
306.42	338.27	4,157.76	0.07	$\delta^{18}O$
310.42	342.53	4,228.86	0.06	$\delta^{13}C$
322.09	354.41	4,373.94	0.08	$\delta^{18}O$
341.00	373.54	4,691.36	0.06	$\delta^{18}O$
353.43	386.12	4,893.50	0.06	$\delta^{13}C$
359.36	392.12	4,975.31	0.07	$\delta^{18}O$
368.25	401.20	5,151.50	0.05	$\delta^{18}O$
378.50	412.03	5,362.40	0.05	K (%) <sup>a</sup>
381.74	415.49	5,437.80	0.05	K (%) <sup>a</sup>
385.83	419.54	5,529.83	0.04	K (%) <sup>a</sup>
388.37	422.07	5,590.28	0.04	K (%) <sup>a</sup>

Note. That the Age Model is Based on the CCSF Depth Scale. IODP, International Ocean Discovery Program.

<sup>a</sup>These tie-points are older than the current new age model and based on the K (%). They are included to allow continuation of the age model toward the Miocene-Pliocene transition and are discussed in detail in Karatsolis et al. (2020).

barriers often lead to diachroneity of biozonal datums compared to apparently global events. One of the better known and more-recent of these regional bio-events is the disappearance of *Globigerinoides ruber* (pink) in the Indo-Pacific realm 120 kyr ago (Thompson et al., 1979), whereas this taxon still lives today in the Atlantic.

Pliocene planktonic foraminiferal biohorizons are mainly calibrated using Pacific or Atlantic studies (Gradstein et al., 2012; King et al., 2020; Wade et al., 2011) and often with differences of up to several 100 kyr (Table 3; Gradstein et al., 2012). These variations hamper the reconstruction of high-resolution paleoceanographic records for the Indian Ocean as it is still unclear which of these biohorizons are applicable to this ocean basin. In addition, existing older biostratigraphic studies for the Indian Ocean (e.g. Srinivasan & Chaturvedi, 1992; Srinivasan & Sinha, 1998; Zachariasse, 1992) are often based on out-of-date age models.

We document 24 early Pliocene to early Pleistocene biostratigraphic datums at IODP Site U1463 that were determined with an average time resolution of ~28 kyr per sample. New ages for the respective biostratigraphic datums are based on the independently, orbitally-tuned benthic isotope age model for IODP Site U1463 (Table 3). The biostratigraphy at IODP Site U1463 can be closely tied to Ocean Drilling Program (ODP) Site 763 further offshore western Australia (Figure 1; Sinha & Singh, 2008). With a few exceptions, the bio-events are very similar at both locations (Table 3). For example, the final occurrence of *Globoturborotalita nepenthes* (4.18 Ma) is ~760 kyr earlier than at ODP Site 763, yet close to the commonly published age (4.38 Ma; King et al., 2020). As *G. nepenthes* is quite rare at IODP Site U1463, its earlier disappearance may be due to specific local oceanographic conditions. Similarly, *Globoconella inflata* appears 670 kyr later at IODP Site U1463 than at ODP Site 763. This species is commonly present in temperate water masses. Accordingly, as *G. inflata* appeared much earlier at ODP Site 763, it implies that this site may have been affected earlier by the north-flowing West Australian Current than the more proximal IODP Site U1463, as was also suggested by previous reconstructions (Auer et al., 2019; De Vleeschouwer et al., 2018; Karas et al., 2011). Some of our Indian Ocean biozonal datums at IODP Site U1463 differ from previous foraminiferal bio-horizons (Table 3; Gradstein et al., 2012; King et al., 2020; Wade et al., 2011). Similar datum variations are also present at ODP Site 763 and IODP Site U1482 on the Scott Plateau further to the northeast (Rosenthal et al., 2018) suggesting that regional conditions resulted in the temporal variation of particular species. The largest difference is the distribution of *Sphaeroidinella dehiscens*, which has a first occurrence at 5.54 Ma (King et al., 2020), yet only appears off northwestern Australia at 3.46 Ma (IODP Site U1463) and 3.58 Ma (ODP Site 763) close to the disappearance of *Sphaeroidinellopsis seminulina* (3.34 Ma) off northwest Australia. Another important bio-event is the last occurrence of *Dentoglobigerina altispira* at 2.68 Ma. This species is commonly present throughout the Miocene and Pliocene and its final occurrence is often assigned to be 3.47 Ma (Gradstein et al., 2012; Wade et al., 2011). However, in several locations in the Pacific and Atlantic it was found to have persisted until 3.11–3.13 Ma (Chaisson and Pearson, 1997; Lourens et al., 2004; Shackleton et al., 1995), and perhaps more commonly into younger strata (Boltovskoy, 1974; Chaisson & Leckie, 1993; Jenkins & Srinivasan, 1986; Lam & Leckie, 2020b; Norris et al., 1998; Shackleton et al., 1995).

Changes in the coiling direction of certain planktonic species such as the genus *Pulleniatina* spp. may be used as biostratigraphic markers (Saito et al., 1976). The most commonly used datum is the L9-event

**Table 3**  
*Biostratigraphic Datums for IODP Site U1463 Based on the New Astronomically-Tuned Age-Depth Model, Geological Timescale, ODP sites 763 and 806B, and First Sample (A/B) Above (Top) or Below (Base) Biostratigraphic Datums, and Variability of the Biostratigraphic Datums*

Marker species	This study <sup>a</sup> Sample	Depth CSF-A (m)	Age (Ma) <sup>b</sup>	A/B sample	Depth CSF-A (m)	Age (Ma)	Midpoint (CSF-A (m))	+ CSF (m)	Ave. Age (Ma)	+ Myr	GTST	ODP Site 763	ODP Site 806B
											Age (Ma) <sup>c</sup>	Age (Ma) <sup>d</sup>	Age (Ma) <sup>e</sup>
Top <i>G. fistulosus</i>	356-U1463C-20H-4-125	178.35	1.685	n.a.	n.a.	n.a.	n.a.	–	–	–	1.88	1.73	1.737
Top <i>G. limbata</i>	356-U1463D-22H-2-85	191.75	1.837	356-U1463D-22H-1-45	189.85	1.813	190.80	1.90	1.825	0.024	2.37	2.10	1.126
Base <i>G. inflata</i>	356-U1463D-22H-6-45	197.35	1.908	356-U1463D-22H-7-45	198.85	1.927	198.10	1.50	1.918	0.019	–	2.58	0.979
Top <i>G. extremus</i>	356-U1463D-23H-3-45	202.35	1.973	356-U1463D-23H-2-5	200.45	1.949	201.40	1.90	1.961	0.024	1.97	1.87	2.172
Top <i>G. exilis</i>	356-U1463C-23H-4-125	206.85	2.039	356-U1463C-23H-3-85	204.95	2.015	205.90	1.90	2.027	0.024	2.08	–	–
Base <i>G. truncatulinoides</i>	356-U1463C-24H-1-125	211.85	2.159	356-U1463C-24H-3-5	213.65	2.184	212.75	1.80	2.171	0.025	1.92	2.10	2.332
Top <i>G. pseudomiocena</i>	356-U1463C-24H-3-5	213.65	2.184	356-U1463C-24H-1-125	211.85	2.159	212.75	1.80	2.171	0.025	2.30	–	4.809
Top <i>G. woodi</i>	356-U1463C-26H-4-5	234.15	2.512	356-U1463C-26H-3-5	232.65	2.488	233.40	1.50	2.500	0.024	2.30	–	2.172
Top <i>D. altispira</i>	356-U1463C-27H-4-125	242.85	2.697	356-U1463C-27H-3-125	241.35	2.670	242.10	1.50	2.683	0.027	3.46 <sup>f</sup> 3.05 <sup>f</sup> 3.00 <sup>f</sup>	3.05	2.603
Base <i>G. tosaensis</i>	356-U1463B-29H-2-89	258.35	3.059	356-U1463B-29H-3-130	260.25	3.109	259.30	1.90	3.084	0.050	3.35	2.84	3.076
Top <i>G. margaritae</i>	356-U1463C-29H-5-42	262.55	3.131	356-U1463C-29H-4-50	261.05	3.200	261.80	1.50	3.165	0.069	3.83	3.38	3.076
Top <i>S. kochi</i>	356-U1463C-29H-5-42	262.55	3.131 <sup>g</sup>	356-U1463C-29H-4-50	261.05	3.200	261.80	1.50	3.165	0.069	4.49	3.35	4.987
Base <i>G. fistulosus</i>	356-U1463B-29H-5-5	262.05	3.155	356-U1463C-29H-4-50	261.05	3.200	261.55	1.00	3.177	0.045	–	3.26	2.801
Top <i>S. seminulina</i>	356-U1463C-30H-2-42	267.55	3.335	356-U1463D-30H-2-9	266.95	3.302	267.25	0.60	3.318	0.033	3.59	3.35	3.625
Top <i>P. primalis</i>	356-U1463C-30H-3-43	269.05	3.358	356-U1463C-30H-2-42	267.55	3.335	268.30	1.50	3.346	0.023	3.66	2.84	2.043
Top <i>G. plesiotumida</i>	356-U1463C-30H-3-43	269.05	3.358	356-U1463C-30H-2-42	267.55	3.335	268.30	1.50	3.346	0.023	3.72	2.39	4.371
Base <i>S. dehiscens</i>	356-U1463B-31F-2-89	273.55	3.445	356-U1463B-31F-3-90	275.05	3.467	274.30	1.50	3.456	0.022	5.54	3.58	4.585
Base <i>G. ruber</i>	356-U1463C-32F-1-130	281.95	3.568	356-U1463C-32F-3-5	283.75	3.598	282.85	1.80	3.583	0.030	–	–	8.704
Base <i>P. obliquiloculata</i>	356-U1463C-32F-3-5	283.75	3.598	356-U1463C-33F-1-45	285.85	3.638	284.80	2.10	3.618	0.040	–	3.33	4.890
Top <i>G. crassula</i>	356-U1463C-37F-1-125	302.95	4.027	356-U1463C-36F-4-5	301.15	3.985	302.05	1.80	4.006	0.042	–	–	5.807
X <i>Pulleniatina</i> sin to dex	356-U1463C-37F-4-45	306.25	4.078	356-U1463C-37F-3-5 <sup>h</sup>	304.75	4.055	305.50	1.50	4.066	0.023	4.06	–	–

**Table 3**  
*continued*

Marker species	This study <sup>a</sup> Sample	Depth		A/B sample	Depth		Midpoint (CSF-A + CSF (m))	Ave. Age (Ma) + Myr	GTST Age (Ma) <sup>c</sup>	ODP Site 763 Age (Ma) <sup>d</sup>	ODP Site 806B Age (Ma) <sup>e</sup>		
		CSF-A (m)	Age (Ma) <sup>b</sup>		CSF-A (m)	Age (Ma)							
Top <i>G. nepenthes</i>	356-U1463C-40F-2-85	314.15	4.200	356-U1463C-40F-1-45	312.25	4.169	313.20	1.90	4.184	0.031	4.38	3.44	4.276
Base <i>G. crassula</i>	356-U1463C-44F-4-5	328.04	4.426	356-U1463C-45F-2-45	330.26	4.466	329.15	2.22	4.446	0.040	–	–	5.898
Base <i>G. crassaformis</i>	356-U1463C-48F-1-45	339.25	4.636	356-U1463C-49F-2-125	342.45	4.697	340.85	3.20	4.666	0.061	4.30	4.41	3.675

IODP, International Ocean Discovery Program

<sup>a</sup>Raw data are available at <https://doi.pangaea.de/10.1594/PANGAEA.921913>. <sup>b</sup>Age based on the new, orbitally-tuned age model for IODP Site U1463. <sup>c</sup>Age as in Wade et al. (2011), Gradstein et al. (2012), and King et al. (2020). <sup>d</sup>Sinha and Singh (2008; ODP Site 763). <sup>e</sup>Lam and Leckie (2020a; ODP Site 806B). <sup>f</sup>3.46 Ma (Wade et al., 2011 - Pacific); 3.05 Ma (Shackleton et al., 1995 - Pacific); 3.11 Ma (Wade et al., 2011 - Atlantic). <sup>g</sup>A similar occurrence was found at IODP Site U1482 (Rosenthal et al., 2018). <sup>h</sup>This is the next sample after %-sinistral specimens was zero for the first time. See text for further discussion.

(100%-sinistral to 100%-dextral) reported at 4.08 Ma (Gallagher et al., 2017; Saito, 1976; Wade et al., 2011). At Site U1463, the first dextral specimens appear at 4.20 Ma and the last sinistral specimens were present at 3.95 Ma, a total time span of ~250 kyr for the full change in coiling direction (Table 3) (see data in Pangaea). After this change *Pulleniatina* disappears from the Atlantic until 2.26 Ma, yet predominantly dextral forms are still present in the Indian Ocean. At IODP Site U1463 sinistral specimens become common and occasionally dominant again after 2.49 Ma and after 1.76 Ma constitute 100% of the specimens equivalent to Saito's events L4–L8.

The Indonesian Throughflow (ITF) is a major influence on the biostratigraphy in the Indian Ocean as it supplies warm waters from the equatorial Pacific. As the ITF is a relatively shallow current system, sub-surface foraminiferal species are living in water masses, which may originate from the sub-Antarctic or even Atlantic rather than from the Pacific. Srinivasan and Sinha (1998) showed that *Pulleniatina spectabilis*, a commonly occurring Pliocene thermocline species in the equatorial Pacific, never migrated into the Indian Ocean during the Pliocene suggesting that the ITF was already restricted to such an extent that only shallower waters may have passed through it. Indeed, *P. spectabilis* is also not present at IODP Site U1463. However, there is no consistent pattern in offsets between biostratigraphic datums for other deeper-dwelling species, especially *Globorotalia* spp. at IODP Site U1463 with those in the Atlantic or the Pacific. Some taxa have ages very similar to Atlantic datums, for example, *Globorotalia exilis*, while others are more similar to Pacific age datums, for example, *Globorotalia pseudomiocenica*, or somewhere in-between, for example *Globorotalia limbata* (Table 3). Although a major switch in the restriction of the ITF occurred 3.5–3.0 Ma when the source waters for the ITF changed from the south Pacific to the north Pacific due to the northward movement of the Australian plate (Cane & Molnar, 2001; Karas et al., 2009), *P. spectabilis* occurred ~5.20–4.20 Ma (Berggren et al., 1995). The lack of a consistent pattern in the biohorizons of deeper-dwelling species during the Pliocene implies that a biogeographical barrier existed prior to the early Pliocene.

One particular biohorizon that may have been established via a different pathway from the Pacific than the ITF is the first occurrence of *Globorotalia truncatulinoides*. This datum is generally placed at 1.93 Ma (Wade et al., 2011), however, in the southwest Pacific this species had already appeared at ~2.8 Ma (Dowsett, 1989; Lazarus et al., 1995; Spencer-Cervato & Thierstein, 1997). At IODP Site U1463, it appears at 2.17 Ma; this may be due to its migration from the southwest Pacific via the Tasman Leakage (Speich et al., 2002; van Sebille et al., 2012).

### 3.3. Correlation of NGR Between IODP Sites and Industry Wells

Time warping the NGR records of the other Exp. 356 IODP sites and industry wells demonstrates that these sequences have similar downhole gamma ray signatures, compared to IODP Site U1463 (Figure 4; Christensen

**Table 4**

*Tie-points (WMSF Depth Scale for IODP Sites; bRT Depth Scale for Industry Wells) for Biostratigraphic Datums at IODP Site U1463 to Other Sites on the NWS*

Marker species	IODP Site U1463			IODP Site U1462		Goodwyn-2	Goodwyn-6	Angel-2	Finucane-1	IODP Site U1464
	Sample	Depth CSF-A (m)	Age (Ma)	Depth WMSF (m)	Depth WMSF (m)	Depth bRT (m)	Depth bRT (m)	Depth bRT (m)	Depth bRT (m)	Depth WMSF (m)
Top <i>G. fistulosus</i>	356-U1463C-20H-4-125	178.35	1.69	173.20	457.96	398.94	447.86	345.15	474.18	79.10
Top <i>G. limbata</i>	356-U1463D-22H-2-85	191.75	1.84	186.72	474.27	420.76	467.40	367.88	500.47	84.89
Base <i>G. inflata</i>	356-U1463D-22H-6-45	197.35	1.91	192.45	484.63	430.71	478.57	379.35	511.94	87.63
Top <i>G. extremus</i>	356-U1463D-23H-3-45	202.35	1.97	197.57	495.60	440.95	487.73	389.58	522.17	90.07
Top <i>G. exilis</i>	356-U1463C-23H-4-125	206.85	2.04	202.18	505.36	449.25	495.45	398.81	531.39	92.20
Base <i>G. truncatulinoides</i>	356-U1463C-24H-1-125	211.85	2.16	207.30	515.42	459.48	503.22	406.75	541.63	94.49
Top <i>G. pseudomiocenica</i>	356-U1463C-24H-3-5	213.65	2.18	209.14	520.14	463.16	506.90	410.13	545.30	95.40
Top <i>G. woodi</i>	356-U1463C-26H-4-5	234.15	2.51	229.61	565.71	503.95	533.97	434.60	586.24	114.45
Top <i>D. altispira</i>	356-U1463C-27H-4-125	242.85	2.70	238.63	592.07	522.00	547.14	451.28	601.67	127.25
Base <i>G. tosaensis</i>	356-U1463B-29H-2-89	258.35	3.06	255.21	630.48	555.14	572.97	478.73	632.87	149.20
Top <i>G. margaritae</i>	356-U1463C-29H-5-42	262.55	3.13	259.55	641.15	563.84	580.60	484.59	641.56	153.92
Top <i>S. kochi</i>	356-U1463C-29H-5-42	262.55	3.13	259.55	641.15	563.84	580.60	484.59	641.56	153.92
Base <i>G. fistulosus</i>	356-U1463B-29H-5-5	262.05	3.16	259.04	639.01	562.80	579.93	483.65	640.53	153.47
Top <i>S. seminulina</i>	356-U1463C-30H-2-42	267.55	3.34	264.58	652.58	573.89	587.51	491.35	651.00	158.50
Top <i>P. primalis</i>	356-U1463C-30H-3-43	269.05	3.36	266.02	657.45	576.77	590.03	492.14	653.27	159.11
Top <i>G. plesiotumida</i>	356-U1463C-30H-3-43	269.05	3.36	266.02	657.45	576.77	590.03	492.14	653.27	159.11
Base <i>S. dehiscens</i>	356-U1463B-31F-2-89	273.55	3.45	270.33	669.80	584.87	594.20	498.03	661.90	163.53
Base <i>G. ruber</i>	356-U1463C-32F-1-130	281.95	3.57	278.39	681.53	596.18	598.22	502.82	673.75	167.79
Base <i>P. obliquiloculata</i>	356-U1463C-32F-3-5	283.75	3.60	280.11	682.60	598.75	599.08	503.68	676.66	168.55
Top <i>G. crassula</i>	356-U1463C-37F-1-125	302.95	4.03	298.44	701.95	621.19	613.45	512.99	691.68	177.55
X <i>Pulleniatina</i> sin to dex	356-U1463C-37F-4-45	306.25	4.08	301.57	703.33	627.46	618.32	515.17	694.37	180.75
Top <i>G. nepenthes</i>	356-U1463C-40F-2-85	314.15	4.20	309.74	709.12	640.95	632.27	519.64	701.96	187.30
Base <i>G. crassula</i>	356-U1463C-44F-4-5	328.04	4.43	324.45	716.89	649.07	640.00	527.07	712.24	195.68
Base <i>G. crassaformis</i>	356-U1463C-48F-1-45	339.25	4.64	335.80	725.27	663.15	651.42	532.75	722.44	202.08

IODP, International Ocean Discovery Program.

et al., 2017). Around the Miocene-Pliocene transition (~5.3 Ma; ~380 m WMSF) an increase in NGR was interpreted by these authors to be related to the onset of a wetter climate in northwestern Australia resulting in an increase in river-brought sediments to the NWS due to increasing precipitation. Although a similar increase is seen at most sites investigated, a recent study suggests that this steep increase may not be solely climate related, but rather a tectonic deepening event that did not occur simultaneously in different basins, although this nevertheless created the accommodation space needed to deposit climate-related cyclic sedimentation (Karatsolis et al., 2020). At IODP Site U1464 located in the Roebuck Basin the onset occurs rather abruptly at ~6.0 Ma (~320 m WMSF), while at Site U1463 in the Northern Carnarvon Basin the onset is later around 5.3 Ma (~380 m WMSF). In addition, all major patterns may be correlated in these different NGR records suggesting a common age history. The uppermost part of the NGR records, that is, above ~80 m, does not show much structure as this part in the NGR signal of the drilling holes is usually impeded by hole casing (Figure 4).

In a final step we projected the biostratigraphic datums determined at IODP Site U1463 onto the other sites following the DTW correlations performed using the NGR. As these correlations are based on U1463

wireline depth below the seafloor (WMSF) and the biostratigraphic datums are reported in U1463 cored depth (CSF-A), this projection involved a conversion of the U1463 depth scale from cored to wireline depth (WMSF). After this conversion, the U1463 biostratigraphic datums were projected along our DTW correlations determining approximate positions of the respective biostratigraphic datums at each site (Table 4). We emphasize that this projection does not classify as a new age model for the other sites but rather predicts the expected position of different biostratigraphic datums.

### 3.4. Seismic Stratigraphic Analyses

A series of 2D multi-channel seismic profiles were combined to produce a regional composite profile across the NWS connecting several IODP 356 sites (Site U1462 to Site U1464) and industry wells over a distance of ~400 km (Figure 6). Tracing of seismic reflectors across large distances such as these often encounters many challenges (e.g. condensed surfaces or erosional truncations) when attempted in isolation. However, integration of seismic data with correlated NGR and biostratigraphical data provides regularly distributed control points that allow for accurate tracing of these horizons, even across uncertain sections. This integration between the NGR, biostratigraphy and seismic data increased the accuracy and absolute age determination of previously published seismic horizons (H6 and H7; Belde et al., 2017; McCaffrey et al., 2020) across the shelf between IODP 356 sites U1462 and U1464. The independent benthic foraminiferal age model constrains the age of seismic reflectors H6 at ~6.2 Ma (408 m WMSF in U1463; previously dated at 5.5 Ma [McCaffrey et al., 2020]) and H7 at 1.89 Ma (191 m WMSF in U1463; previously dated at 3-2.5 Ma [McCaffrey et al., 2020]) (Belde et al., 2017; McCaffrey et al., 2020; Rosleff-Soerensen et al., 2012).

The transition from the Miocene into the Pliocene is represented across the majority of the shelf between IODP sites U1462 and U1464 by the distinct shift in reflector geometry. This transition, from sets of strong reflectors surrounded by discontinuous zones of disrupted reflectors below the H6 horizon (~6.2 Ma, Figure 6), to low amplitude parallel reflectors above, is observed in the well data as a shift in lithology from shallow water carbonate/reefal dominated, to deeper water fine grained sediments. Toward the southern end of the section, the seismic architecture becomes increasingly complex as these sediments are interbedded with the mixed siliciclastic and carbonate Bare Formation (Figure 6). This unit developed as a fluvial to fluvio-deltaic deposit on a mainly carbonate-dominated shelf (Cathro et al., 2003; Sanchez et al., 2012; Tagliaro et al., 2018; Wallace et al., 2003). Siliciclastic input became especially intense from the Pliocene onwards when climate became wetter (Christensen et al., 2017). Between IODP Site U1462 and Angel-2 the Plio-Pleistocene sediments are observed to be underlain by the Bare Formation, placing the top of the Bare Formation at 5.59 Ma at IODP Site U1462. Further north however, between Angel-2 and Finucane-1, a thick siliciclastic package ending at ~2.38 Ma is observed to be interbedded with the surrounding Plio-Pleistocene sediments, showing that this formation is non-synchronously deposited along the NWS (Figure 6). Tagliaro et al. (2018) even identified Bare-like sediments within the overlying carbonates at the nearby industry well Bounty-1 with an age of 1.63 Ma, although the sand layers were minor in comparison with the limestone surrounding them.

Further toward the northeast the Cenozoic sediment sequence of predominantly carbonates continues further back in time until the early Cenozoic, although IODP sites U1463 and U1464 only drilled to the early Miocene (Gallagher et al., 2017; Groeneveld et al., 2017). The depositional setting during the Miocene is generally very shallow with likely subaerial exposure during certain times such that hiatuses may be present (Groeneveld et al., 2017; Petrick et al., 2019).

Additionally, a dip profile crossing the Northern Carnarvon Basin at the location of IODP Site U1463 was constructed showing the general downslope geometry of the shelf (Figure 7). This profile also shows reef developments during the Miocene, and the presence of a newly identified mass transport deposit on top of the regular sedimentary sequence, called the Picard-slide (Gallagher et al., 2017; Figure 7) with an estimated age range between 910 and 610 ka.

### 3.5. Implications for Dating the History of the NWS

The creation of a consistent age model for the late Neogene strata on the NWS and its relationship to other subsurface downhole and seismic datasets has allowed us to produce a consistent framework to investigate

the evolution of various laterally discontinuous carbonate (tropical reefs) and siliciclastic (the Bare Formation) units that are widespread in this region. After large areas of the NWS were sub-aerially exposed during the late Miocene (Groeneveld et al., 2017; Petrick et al., 2019; Tagliaro et al., 2018), tectonic subsidence during the latest Miocene created sufficient accommodation space to deposit a thick sequence of sediments during the Pliocene and early Pleistocene (Gallagher et al., 2017; Gurnis et al., 2020). This tectonic subsidence is also thought to play a role in the transition of the NWS reef system from primarily barrier reef morphologies in the middle Miocene to pinnacle and atoll formations in the Pliocene (McCaffrey et al., 2020). Our new age framework suggests that deposition of the siliciclastic Bare Formation occurred during the late Miocene and early Pliocene. The Bare Formation is a laterally discontinuous progradational sand-dominated unit that reached IODP Site U1462 by the earliest Pliocene (Tagliaro et al., 2018). Deposition of the Bare Formation expanded and prograded with the onset of wet climate in northwestern Australia near the base of the Pliocene (5.3 Ma), and deposition continued until climate switched again to dry conditions by the early Pleistocene (2.39–1.93 Ma; Christensen et al., 2017; Tagliaro et al., 2018). Our new age framework constrains the age of the termination of this siliciclastic pulse to 2.38 Ma (222 m WMSF in U1463) near Angel-2 (Figure 6), with remnant siliciclastic deposition continuing until as young as 1.63 Ma at the nearby industry well Bounty-1 (Tagliaro et al., 2018).

Our age constrained seismic stratigraphic framework may be applied to most of continental shelf and slope regions of the NWS over an area of  $\sim 150,000$  km<sup>2</sup>. Paleooceanographic drilling has been performed for example on the Wombat Plateau located north of the NWS providing reconstructions going back to the early Cenozoic, but also including detailed studies on the Pliocene and Pleistocene (Exon et al., 1992; Holbourn et al., 2004; Karas et al., 2011). More recently IODP Expedition 363 drilled sites U1482 and U1483 off the northwestern slope of the NWS in the direct outflow of the Indonesian Gateway (Rosenthal et al., 2018). However, linking these dated reflectors to deep ocean archive is not straightforward as deep ocean to continental margin linking seismic data are rare. Nevertheless, the NGR and benthic isotope records of the NWS can be correlated allowing a direct link between pelagic paleooceanographic reconstructions and the terrestrial input from Australia to the more proximal locations.

#### 4. Conclusions

In this study, we have created a high-resolution regional framework to precisely determine the ages of sediments and events on the northwest shelf (NWS) of Australia. This area is ideally located to record changes in the outflow of the Indonesian Throughflow (ITF) as well as to monitor how monsoonal precipitation and aridity change over Australia.

We reconstructed an independent, astronomically tuned age model based on benthic foraminiferal oxygen and carbon isotopes for International Ocean Discovery Program (IODP) Site U1463. The NGR record for IODP Site U1463 was then correlated to the NGR records of several other IODP sites and industry wells on the NWS. Additionally, these sites were linked to each other using a composite seismic profile along the NWS connecting the main reflectors in the region.

This independently dated and consistent age framework for the NWS allowed us to update existing biostratigraphic datums on planktonic foraminifera, and to fine-tune the ages of the main seismic reflectors and major sedimentary events, for example, top of the Bare Formation at 2.38 Ma, on the NWS. Biostratigraphic datums of deeper-dwelling planktonic foraminifera show that the ITF shoaled sufficiently near the start of the Pliocene to act as biogeographical barrier. Comparison with regional (ODP Site 763A and IODP Site U1482) and global biostratigraphic events suggests that this area may have provided specific conditions such that some species, that is, *D. altispira*, *Sphaeroidinellopsis kochi*, and *Globorotalia margaritae*, survived several 100 kyr longer than their published last occurrences in the tropical to subtropical biozonation scheme (King et al., 2020; Wade et al., 2011).

We showed how the combination between an independent orbitally-tuned benthic isotope record, down-hole records of physical properties and an extensive seismic network, a framework can be created that provides a consistent age model for a specific region. This regional and seismically tied Neogene age model can be used to improve age constraints on subsurface reef and carbonate platform development (e.g., McCaffrey

et al., 2020), mass transport deposit generation and periodicity, and the evolution of major siliciclastic pulses (e.g. the Bare Formation; Tagliaro et al., 2018) related to regional (and global) climate and oceanic events.

### Data Availability Statement

Data are stored in the Pangaea database (<https://doi.pangaea.de/10.1594/PANGAEA.921913>). The R-code used for dynamic time warping can be found on Zenodo (<https://doi.org/10.5281/zenodo.4311184>).

### Acknowledgments

The authors thank Henning Kuhnert for laboratory assistance, and Julia Windsberger and Nele Behrendt for assistance with sample processing. This project was supported by the German Academic Exchange Service (DAAD Project "DANA" ID 57388289 to J. Groeneveld, D. De Vleeschouwer, J. McCaffrey, and S. J. Gallagher), and the German Research Foundation (DFG Project "IDEAL" GR 3528/5-1 to J. Groeneveld). Additional funding to S. J. Gallagher was provided by the Australian IODP office and the ARC Basins Genesis Hub (IH130200012). An Australian Government Research Training Program Scholarship is supporting J.C. McCaffrey. The authors would like to thank the IHS Markit for their donation of the Kingdom seismic interpretation software. This research used samples and data provided by the IODP. The authors thank the JRSO (JOIDES Resolution Science Operator) staff and the Siem Offshore crew for their invaluable assistance and skill during Expedition 356. The authors thank editor Adina Paytan, one anonymous reviewer and Adriane Lam for their constructive reviews of the manuscript.

### References

Anell, I., & Wallace, M. W. (2019). A fine balance: Accommodation dominated control of contemporaneous cool-carbonate shelf-edge clinoforms and tropical reef-margin trajectories, North Carnarvon Basin, NW Australia. *Sedimentology*, 67, 96–117. <https://doi.org/10.1111/sed.12628>

Auer, G., De Vleeschouwer, D., Smith, R., Bogus, K. A., Groeneveld, J., Grunert, P., et al. (2019). Timing and pacing of Indonesian Throughflow restriction to Late Pliocene climate shifts. *Paleoceanography and Paleoclimatology*, 34, 635–657. <https://doi.org/10.1029/2018PA003512>

Belde, J., Back, S., Bourget, J., & Reuning, L. (2017). Oligocene and Miocene carbonate platform development in the Browse Basin, Australian Northwest shelf. *Journal of Sedimentary Research*, 87, 795–816. <https://doi.org/10.2110/jsr.2017.44>

Berggren, W. A., Hilgen, F. J., Langereis, C. G., Kent, D. V., Obradovic, J. D., Raffi, I., et al. (1995). Late Neogene chronology: New perspectives in high-resolution stratigraphy. *GSA Bulletin*, 107, 1272–1287.

Bolli, H. M., & Saunders, J. B. (1985). Oligocene to Holocene low latitude planktonic foraminifera. In H. M. Bolli, J. B. Saunders, & K. Perch-Nielsen (Eds.), *Plankton stratigraphy (Vol. 1): Planktic foraminifera, calcareous nannofossils and calpionellids* (pp. 155–262). Cambridge: Cambridge University Press.

Boltovskoy, E. (1974). Neogene planktonic foraminifera of the Indian Ocean (DSDP Leg 26). In T. A. Davies & B. P. Luyendyk (Eds.), *Initial reports of the deep sea drilling project (Vol. 26 pp. 675–741)*. Washington, DC: US Government Printing Office.

Bronk Ramsey, C. (2009). Dealing with outliers and offsets in radiocarbon dating. *Radiocarbon*, 51(3), 1023–1045.

Cane, M., & Molnar, P. (2001). Closing of the Indonesian seaway as a precursor to east African aridification around 3–4 million years ago. *Nature*, 411, 157–162. <https://doi.org/10.1038/35075500>

Cathro, D. L., Austin, J. A. J. R., & Moss, G. D. (2003). Progradation along a deeply submerged Oligocene-Miocene heterozoan carbonate shelf: How sensitive are clinoforms to sea level variations? *American Association Petrology and Geology Bulletin*, 87, 1547–1574.

Chaisson, W. P., & Leckie, R. M. (1993). High-resolution Neogene planktonic foraminifer biostratigraphy of Site 806, Ontong Java Plateau (western equatorial Pacific). In W. H. Berger, L. W. Kroenke, & L. A. Mayer (Eds.), *Proceedings of the Ocean Drilling Program. Scientific Results (Vol. 130, pp. 137–178)*. College Station, TX (ODP).

Chaisson, W. P., & Pearson, P. N. (1997). Planktonic foraminifer biostratigraphy at Site 925: Middle Miocene to Pleistocene. In N. J. Shackleton, W. B. Curry, C. Richter, & T. J. Bralower (Eds.), *Proceedings of the Ocean Drilling Program. Scientific Results (Vol. 154 pp. 3–31)*. College Station, TX (ODP).

Christensen, B. A., Renema, W., Henderiks, J., De Vleeschouwer, D., Groeneveld, J., Castañeda, I. S., Reuning, L., et al. (2017). Indonesian Throughflow drove Australian climate from humid Pliocene to arid Pleistocene. *Geophysical Research Letters*, 44, 6914–6925. <https://doi.org/10.1002/2017GL072977>

Cleveland, W. S. (1979). Robust locally weighted regression and smoothing scatterplots. *Journal of the American Statistical Association*, 74, 829–836. <https://doi.org/10.1080/01621459>

Collins, L. B. (2002). Tertiary foundations and Quaternary evolution of coral reef systems of Australia's North West Shelf. In M. Keep & S. J. Moss (Eds.), *The sedimentary basins of western Australia 3: Proceedings of petroleum exploration society of Australia symposium (pp. 129–152)*. Perth: Petroleum Exploration Society of Australia.

De Vleeschouwer, D., Auer, G., Smith, R., Bogus, K. A., Christensen, B. A., Groeneveld, J., et al. (2018). The amplifying effect of Indonesian Throughflow heat transfer on Late Pliocene southern Hemisphere climate cooling. *Earth and Planetary Science Letters*, 500, 15–27. <https://doi.org/10.1016/j.epsl.2018.07.0350012-821X>

De Vleeschouwer, D., Petrick, B. F., & Martínez-García, A. (2019). Stepwise weakening of the Pliocene Leeuwin current. *Geophysical Research Letters*, 46(14), 8310–8319.

De Vleeschouwer, D., Vahlenkamp, M., Crucifix, M., & Pälike, H. (2017). Alternating Southern and Northern Hemisphere climate response to astronomical forcing during the past 35 m.y. *Geology*, 45(4), 375–378. <https://doi.org/10.1130/G386663.1>

Dowsett, H. J. (1989). Application of the graphic correlation method to Pliocene marine sequences. *Marine Micropaleontology*, 14, 3–32.

Exon, N. F., Borella, P. E., & Ito, M. (1992). Sedimentology of marine Cretaceous sequences in the central Exmouth Plateau (northwest Australia). In U. von Rad, B. U. Haq, et al. (Eds.), *Proceedings of the Ocean Drilling Program (Vol. 122 pp. 233–257)*. Scientific Results.

Gallagher, S. J., & deMenocal, P. B. (2019). Finding dry spells in Ocean sediments. *Oceanography*, 32(1), 38–41. <https://doi.org/10.5670/oceanog.2019.120>

Gallagher, S. J., Fulthorpe, C. L., Bogus, K. A., Auer, G., Baranwal, S., Castañeda, I. S., et al. (2017). Indonesian Throughflow. *Proceedings of the International Ocean Discovery Program*, 356, 1–43. <https://doi.org/10.14379/iodp.proc.356.101.2017>

Gallagher, S. J., Reuning, L., Himmler, T., Henderiks, J., De Vleeschouwer, D., Groeneveld, J., et al. (2018). The enigma of rare Quaternary oolites in the Indian and Pacific Oceans: A result of global oceanographic physicochemical conditions or a sampling bias. *Quaternary Science Reviews*, 200, 114–122. <https://doi.org/10.1016/j.quascirev.2018.09.028>

Gallagher, S. J., Wallace, M. W., Hoiles, P. W., & Southwood, J. M. (2014). Seismic and stratigraphic evidence for reef expansion and onset of aridity on the Northwest Shelf of Australia during the Pleistocene. *Marine and Petroleum Geology*, 57, 470–481.

Gallagher, S. J., Wallace, M. W., Li, C. L., Kinna, B., Bye, J. T., Akimoto, K., & Torii, M. (2009). Neogene history of the West Pacific warm pool, Kuroshio and Leeuwin currents. *Paleoceanography*, 24, PA1206. <https://doi.org/10.1029/2008PA001660>

Giorgino, T. (2009). Computing and visualizing dynamic time warping alignments in R: The DTW package. *Journal of Statistical Software*, 31(7), 1–24.

Goktas, P., Austin, J. A., Fulthorpe, C. S., & Gallagher, S. J. (2016). Morphologies and depositional/erosional controls on evolution of Pliocene-Pleistocene carbonate platforms: Northern Carnarvon Basin, Northwest Shelf of Australia. *Continental Shelf Research*, 124, 63–82. <https://doi.org/10.1016/j.csr.2016.05.009>

- Gorter, J. D., Rexilius, J. P., Powell, S. L., & Bayford, S. W. (2002). Late early to mid-Miocene patch reefs, Ashmore Platform, Timor sea; evidence from 2D and 3D seismic surveys and petroleum exploration wells. In M. Keep & S. J. Moss (Eds.), *The sedimentary basins of western Australia 3: Proceedings of petroleum exploration society of Australia symposium* (pp. 355–376). Perth: Petroleum Exploration Society of Australia.
- Gradstein, F. M., Ogg, J. G., Schmitz, M., & Ogg, G. (2012). In *The Geologic Time Scale 2012* (Vol. 1, p. 435). Elsevier.
- Groeneveld, J., Henderiks, J., Renema, W., McHugh, C. M., De Vleeschouwer, D., Christensen, B. A., et al. (2017). 356 Scientists Australian shelf sediments reveal shifts in miocene Southern hemisphere westerlies. *Science Advances*, 3, e1602567.
- Gurnis, M., Kominz, M., & Gallagher, S. J. (2020). Reversible subsidence on the North West Shelf of Australia. *Earth and Planetary Science Letters*, 534, 116070.
- Hengesh, J. V., Dirstein, J. K., & Stanley, A. J. (2013). Landslide geomorphology along the Exmouth Plateau continental margin, North West Shelf, Australia. *Australian Geomechanics Journal, Special Offshore Edition*, 48(4), 71–92.
- Hilgen, F., Lourens, L., Pälike, H., & Dinarès Turell, J. (2020). Should Unit-Stratotypes and Astrochronozones be formally defined? A dual proposal (including postscriptum). *Newsletters on Stratigraphy*, 53, 19–39. <https://doi.org/10.1127/nos/2019/0514>
- Holbourn, A., Kuhnt, W., Simo, J. A., & Li, Q. (2004). Middle Miocene isotope stratigraphy and paleoceanographic evolution of the north-west and southwest Australian margins (Wombat Plateau and Great Australian Bight). *Palaeogeography, Palaeoclimatology, Palaeoecology*, 208, 1–22.
- Huybers, P., & Wunsch, C. (2004). A depth-derived Pleistocene age model: Uncertainty estimates, sedimentation variability, and nonlinear climate change. *Paleoceanography*, 19, PA1028. <https://doi.org/10.1029/2002PA000857>
- Ishiya, T., Yokoyama, Y., Reuning, L., McHugh, C. M., De Vleeschouwer, D., & Gallagher, S. J. (2019). Australian summer monsoon variability in the past 14,000 years revealed by IODP Expedition 356 sediments. *Progress in Earth and Planetary Science*, 6, 1–17. <https://doi.org/10.1186/s40645-019-0262-5>
- James, N. P., Bone, Y., Kyser, T. K., Dix, G. R., & Collins, L. B. (2004). The importance of changing oceanography in controlling late Quaternary carbonate sedimentation on a high-energy, tropical, oceanic ramp: North-western Australia. *Sedimentology*, 51, 1179–1205.
- Jenkins, D. G., & Srinivasan, M. S. (1986). Cenozoic planktonic foraminifers from the equator to the sub-Antarctic of the southwest Pacific. In J. P. Kennett, & C. C. von der Borch (Eds.), *Initial Reports of the deep sea drilling project*, (Vol. 90, pp. 795–834). Washington, DC: US Government Printing Office.
- Jones, H. A. (1973). Marine geology of the northwest Australian continental shelf. Bureau of mineralogical resources. *Geological and Geophysical Bulletin*, 136, 1A–102A.
- Karas, C., Nürnberg, D., Gupta, A. K., Tiedemann, R., Mohan, K., & Bickert, T. (2009). Mid-Pliocene climate change amplified by a switch in Indonesian subsurface throughflow. *Nature Geoscience*, 2, 434–438.
- Karas, C., Nürnberg, D., Tiedemann, R., & Garbe-Schonberg, D. (2011). Pliocene Indonesian Throughflow and Leeuwin Current dynamics: Implications for Indian Ocean polar heat flux. *Paleoceanography*, 26. <https://doi.org/10.1029/2010pa001949>
- Karatsolis, B. T., De Vleeschouwer, D., Groeneveld, J., Christensen, B., & Henderiks, J. (2020). The late Miocene–early Pliocene “Humid Interval” on the NW Australian shelf: Disentangling climate forcing from regional basin evolution. *Paleoceanography and Paleoclimatology*, 35, e2019PA003780. <https://doi.org/10.1029/2019PA003780>
- Keep, M., Holbourn, A., Kuhnt, W., & Gallagher, S. J. (2018). Progressive Western Australian collision with Asia: Implications for regional oceanography, oceanography, climate and marine biota. *Journal of the Royal Society of Western Australia*, 101, 1–17.
- Kennett, J. P., & Srinivasan, M. S. (1983). *Neogene planktonic foraminifera: A phylogenetic atlas* (p. 263). Stroudsburg, PA: Hutchison Ross.
- King, D. J., Wade, B. S., Liska, R. D., & Miller, C. G. (2020). A review of the importance of the Caribbean region in Oligo-Miocene low latitude planktonic foraminiferal biostratigraphy and the implications for modern biogeochronological schemes. *Earth-Science Reviews*, 202, 102968.
- Kotov, S., & Pälike, H. (2017). MyDTW-Dynamic time warping program for stratigraphical time series. *Proceedings 19th EGU General Assembly, EGU2017*, 23–28 April, 2017 (p. 2157). Vienna, Austria.
- Lam, A. R., & Leckie, R. M. (2020a). Late Neogene and quaternary diversity and taxonomy of subtropical to temperate planktic foraminifera across the Kuroshio current Extension, northwest Pacific Ocean. *Micropaleontology*, 66(3), 177–268.
- Lam, A. R., & Leckie, R. M. (2020b). Subtropical to temperate late Neogene to Quaternary Planktic foraminiferal biostratigraphy across the Kuroshio current extension, Shatsky Rise, northwest Pacific. *PLoS One*, 15. <https://doi.org/10.1371/journal.pone.0234351>
- Laskar, J., Robutel, P., Joutel, F., Gastineau, M., Correia, A., & Levrard, B. (2004). A long-term numerical solution for the insolation quantities of the Earth. *Astronomy and Astrophysics*, 428, 261–285.
- Lazarus, D., Hilbrecht, H., Spencer-Cervato, C., & Thierstein, H. R. (1995). Sympatric speciation and phyletic change in Globorotalia truncatulinoides. *Paleobiology*, 21, 28–51.
- Lisiecki, L. E., & Herbert, T. D. (2007). Automated composite depth scale construction and estimates of sediment core extension. *Paleoceanography*, 22(4). <https://doi.org/10.1029/2006PA001401>
- Lisiecki, L. E., & Lisiecki, P. A. (2002). Application of dynamic programming to the correlation of paleoclimate records. *Paleoceanography*, 17(4), 1049. <https://doi.org/10.1029/2001PA000733>
- Lisiecki, L. E., & Raymo, M. E. (2005). A Pliocene-Pleistocene stack of 57 globally distributed benthic  $\delta^{18}\text{O}$  records. *Paleoceanography*, 20, PA1003. <https://doi.org/10.1029/2004PA001071>
- Longley, I. M., Buessenschuett, C., Clydsdale, L., Cubitt, C. J., Davis, R. C., Johnson, M. K., et al. (2002). The North West Shelf of Australia—A Woodside perspective. In M. Keep, & S. J. Moss (Eds.), *The Sedimentary Basins of Western Australia 3* (pp. 27–88). Proceedings of the Petroleum Exploration Society of Australia Perth.
- Lourens, L. J., Hilgen, F. J., Laskar, J., Shackleton, N. J., & Wilson, D. (2004). The Neogene period. In F. Gradstein, J. Ogg, & A. G. Smith (Eds.), *A geological time scale 2004* (pp. 409–440). Cambridge: Cambridge University Press.
- McCaffrey, J., Wallace, M. W., & Gallagher, S. J. (2020). A Cenozoic Great Barrier Reef on Australia's North West Shelf. *Global and Planetary Change*, 184, 1030148. <https://doi.org/10.1016/j.gloplacha.2019.103048>
- Meyers, S. R. (2012). Seeing red in cyclic stratigraphy: Spectral noise estimation for astrochronology. *Paleoceanography*, 27, PA3228. <https://doi.org/10.1029/2012PA002307>
- Meyers, S. R. (2014). *Astrochron: An R package for astrochronology*.
- Mitchum, R. M., Jr, Vail, P. R., & Sangree, J. B. (1977). Seismic stratigraphy and global changes of sea level, part 6: Stratigraphic interpretation of seismic reflection patterns in depositional sequences. *Seismic Stratigraphy—Application to Hydrocarbon Exploration*, 165, 117–134. <https://doi.org/10.1038/272400a0>
- Moss, G. D., Cathro, D. L., & Austin, J. A., Jr. (2004). Sequence biostratigraphy of prograding clinoforms, northern Carnarvon Basin, Western Australia: A proxy for variations in Oligocene to Pliocene global sea level? *Palaios*, 19, 206–226.

- Norris, R. D. (1998). Planktonic foraminifer biostratigraphy: Eastern equatorial Atlantic, Leg 159. In J. Mascle, G. P. Lohmann, & M. Moullade (Eds.), *Proceedings of the Ocean Drilling Program. Scientific Results* (Vol. 159, pp. 445–479). College Station, TX
- Patrick, B., Reuning, L., & Martinez-Garcia, A. (2019). Distribution of glycerol dialkyl glycerol tetraethers (GDGTs) in microbial mats from Holocene and Miocene Sabkha sediments. *Frontiers in Earth Science*, 7(310). <https://doi.org/10.3389/feart.2019.00310>
- Power, M. (2008). Miocene carbonate reef complexes in the Browse Basin and the implication for drilling operations. *Australian Petroleum Production and Exploration Association Journal*, 48, 115–132.
- R Core Team. (2014). *R: A language and environment for statistical computing*. Vienna: R Foundation for Statistical Computing.
- Rosenthal, Y., Holbourn, A. E., Kulhanek, D. K., Aiello, I. W., Babila, T. L., Bayon, G., et al. (2018). Expedition 363. In Y. Rosenthal, A. E. Holbourn, & D. K. Kulhanek (Eds.), *The Expedition 363 Scientists, Western Pacific Warm Pool. Proceedings of the International Ocean Discovery Program* (Vol. 363). International Ocean Discovery Program, College Station, TX. <https://doi.org/10.14379/iop.proc.363.101.2018>
- Rosleff-Soerensen, B., Reuning, L., Back, S., & Kukla, P. (2012). Seismic geomorphology and growth architecture of a Miocene barrier reef, Browse Basin, NW-Australia. *Marine and Petroleum Geology*, 29, 233–254.
- Ruckstuhl, A. F., Jacobson, M. P., Field, R. W., & Dodd, J. A. (2001). Baseline subtraction using robust local regression estimation. *Journal Quantitative Spectroscopy Radiative Transfer*, 68, 179–193. [https://doi.org/10.1016/S0022-4073\(00\)00021-2](https://doi.org/10.1016/S0022-4073(00)00021-2)
- Ryan, G. J., Bernardel, G., Kennard, J. M., Jones, A. T., Logan, G. A., & Rollet, N. (2009). A precursor extensive Miocene reef system to the Rowley Shoals reefs, WA: Evidence for structural control of reef growth or natural hydrocarbon seepage. *Australian Petroleum Production and Exploration Association Journal*, 49, 337–363.
- Saito, T. (1976). Geologic significance of coiling direction in the planktonic foraminifer *Pulleniatina*. *Geology*, 4(5), 305–309.
- Sakoe, H., & Chiba, S. (1978). Dynamic programming algorithm optimization for spoken word recognition. *IEEE Transactions on Acoustics, Speech, and Signal Processing*, 26(1), 43–49. <https://doi.org/10.1109/TASSP.1978.1163055>
- Sanchez, C. M., Fulthorpe, C. S., & Steel, R. J. (2012). Middle Miocene–Pliocene siliciclastic influx across a carbonate shelf and influence of deltaic sedimentation on shelf construction, Northern Carnarvon Basin, Northwest Shelf of Australia. *Basin Research*, 24, 664–682.
- Scarselli, N., McClay, K., & Elders, C. (2013). Submarine slide and slump complexes, Exmouth Plateau, NW Shelf of Australia. In M. Keep, & S. J. Moss (Eds.), *The Sedimentary Basins of Western Australia 3, Proceedings of the Petroleum* (pp. 1–20). Australia: Exploration Society of Australia Perth.
- Schiebel, R., & Hemleben, C. (2017). *Planktic foraminifers in the modern ocean* (p. 358). Springer-Verlag Berlin Heidelberg.
- Shackleton, N. J., Baldauf, J. G., Flores, J.-A., Iwai, M., Moore, T. C., Jr, Raffi, I., & Vincent, E. (1995). Biostratigraphic summary for Leg 138. In N. G. Pisias, L. A. Mayer, T. R. Janacek, et al. (Eds.), *Proceedings of the Ocean Drilling Program. Scientific Results* (Vol. 138, pp. 517–536). College Station, TX: Ocean Drilling Program.
- Sinha, D. K., & Singh, A. K. (2008). Late Neogene planktic foraminiferal biochronology of the ODP Site 763A, Exmouth Plateau, southeast Indian Ocean. *Journal of Foraminiferal Research*, 38, 251–270.
- Sinnesael, M., De Vleeschouwer, D., Zeeden, C., Batenburg, S. J., Da Silva, A. C., de Winter, N. J., & Hinnov, L. A. (2019). The Cyclostratigraphy Intercomparison Project (CIP): Consistency, merits and pitfalls. *Earth-Science Reviews*, 199, 102965.
- Smith, R. A., Castañeda, I. S., Henderiks, J., Christensen, B. A., De Vleeschouwer, D., Renema, W., et al. (2020). Plio-Pleistocene Indonesian Throughflow variability drove eastern Indian Ocean sea surface temperatures. *Paleoceanography and Paleoclimatology*, 35, e2020PA003872. <https://doi.org/10.1029/2020PA003872>
- Speich, S., Blanke, B., de Vries, P., Drijfhout, S., Döös, K., Ganachaud, A., & Marsh, R. (2002). Tasman leakage: A new route in the global ocean conveyor belt. *Geophysical Research Letters*, 29, 55–51. <https://doi.org/10.1029/2001GL014586>
- Spencer-Cervato, C., & Thierstein, H. R. (1997). First appearance of *Globorotalia truncatulinoides*: Cladogenesis and immigration. *Marine Micropaleontology*, 30, 267–291.
- Srinivasan, M. S., & Chaturvedi, S. N. (1992). Neogene planktonic foraminiferal biochronology of the DSDP sites along the Ninetyeast Ridge, northern Indian Ocean. In K. Ishizaki, & T. Saito (Eds.), *Centenary of Japanese micropaleontology* (pp. 175–188).
- Srinivasan, M. S., & Sinha, D. K. (1998). Early Pliocene closing of the Indonesian Seaway: Evidence from north-east Indian Ocean and tropical Pacific deep sea cores. *Journal of Asian Earth Sciences*, 16, 29–44.
- Tagliaro, G., Fulthorpe, C., Gallagher, S., McHugh, C., Kominz, M., & Lavier, L. (2018). Neogene siliciclastic deposition and climate variability on a carbonate margin: Australian Northwest Shelf. *Marine Geology*, 403, 285–300.
- Thompson, P. R., Bé, A. W. H., Duplessy, J.-C., & Shackleton, N. J. (1979). Disappearance of pink-pigmented *Globigerinoides ruber* at 120,000 yr BP in the Indian and Pacific oceans. *Nature*, 280, 554–558.
- Thomson, D. J. (1982). Spectrum estimation and harmonic analysis. *Proceedings of the IEEE*, 70, 1055–1096.
- Van Sebille, E., England, M. H., Zika, J. D., & Sloyan, B. M. (2012). Tasman Leakage in a fine-resolution ocean model. *Geophysical Research Letters*, 39. <https://doi.org/10.1029/2012gl051004>
- Wade, B. S., Olsson, R. K., Pearson, P. N., Huber, B. T., & Berggren, W. A. (2018). In *Atlas of Oligocene planktonic foraminifera* (Vol. 46, p. 528). Cushman Foundation for Foraminiferal Research, Special Publication.
- Wade, B. S., Pearson, P. N., Berggren, W. A., & Pälike, H. (2011). Review and revision of Cenozoic tropical planktonic foraminiferal biostratigraphy and calibration to the geomagnetic polarity and astronomical time scale. *Earth-Science Reviews*, 104, 111–142.
- Wallace, M. W., Condilis, E., Powell, A., Redfearn, J., Auld, K., Wiltshire, M., & Gallagher, S. J. (2003). Geological controls on sonic velocity in the Cenozoic carbonates of the Northern Carnarvon Basin, North West Shelf, Western Australia. *Australian Petroleum Production and Exploration Association Journal*, 43, 385–399.
- Zachariasse, W. J. (1992). Neogene planktonic foraminifers from Sites 761 and 762 off northwest Australia. In *Proceedings of the Ocean Drilling Program. Scientific Results* (Vol. 122, pp. 665–681).
- Zachos, J. C., Pagani, M., Sloan, L., Thomas, E., & Billups, K. (2001). Trends, rhythms, and aberrations in global climate 65 Ma to present. *Science*, 292, 686–693. <https://doi.org/10.1126/science.1059412>